Structural evolution in Pt/Ga-Zn-oxynitride catalysts for photocatalytic reforming of methanol

Materials Research Bulletin, Volume 83, November 2016, Pages 65-76

Ádám Vass, Zoltán Pászti, Szabolcs Bálint, Péter Németh, Gábor P. Szíjjártó, András Tompos, Emília Tálas

http://dx.doi.org/10.1016/j.materresbull.2016.05.012

ISSN: 00255408 CODEN: MRBUA Source Type: Journal Original language: English

DOI: 10.1016/j.materresbull.2016.05.012 Document Type: Article

Publisher: Elsevier Ltd

Corresponding author: Emília Tálas

Graphical abstract:

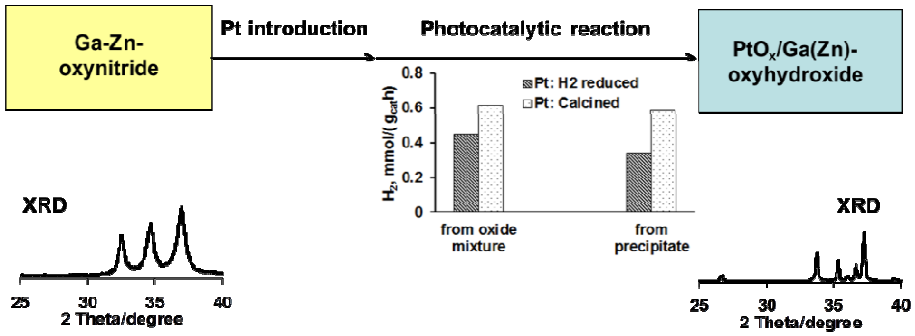

Structural evolution in Pt/Ga-Zn-oxynitride catalysts for photocatalytic reforming of methanol

Ádám Vass, Zoltán Pászti, Szabolcs Bálint, Péter Németh, Gábor P. Szíjjártó, András Tompos, Emília Tálas*

Institute of Materials and Environmental Chemistry, Research Centre for Natural Sciences, Hungarian Academy of Sciences, H-1117 Budapest, Magyar tudósok körútja 2, Hungary

*Corresponding author, Tel.: +36 1 382 6916, email: talas.emilia@ttk.mta.hu, address: H-1519 Budapest, P.O.Box 286, Hungary (Emília Tálas)

Abstract

Products of microwave-assisted urea-induced co-precipitation of $Ga(NO_3)_3$ and $Zn(NO_3)_2$ or Ga_2O_3 and ZnO were nitridated in order to obtain Ga-Zn-based photocatalysts. Irrespectively to the starting material, wurtzite-like Ga-Zn-oxynitride phases formed. The preparation was completed by deposition of a Pt co-catalyst, which was activated by either reduction in hydrogen or calcination in air. It was demonstrated by X-ray diffraction (XRD), transmission electron microscopy (TEM) and X-ray photoelectron spectroscopy (XPS) that during oxidative activation the oxynitride started to transform into a nitrogen-free Zn-containing Ga-oxyhydroxide. Regardless to the structure of the catalysts after the activation step, almost complete oxynitride to oxyhydroxide transformation was observed during the methanol photocatalytic reforming reaction, accompanied by complete reduction of the Pt co-catalyst to metallic state. The observations of this study point to the importance of phase transitions under reaction conditions in the development of the active ensemble in the Ga,Zn-based photocatalysts.

Keywords: A.nitrides; C.X-ray diffraction; C.photoelectron spectroscopy; D.catalytic properties; D.surface properties

Introduction

Photocatalytic hydrogen production is a promising approach for storing solar energy in chemical form. High gravimetric energy density, abundance and storage potential make hydrogen a potential energy carrier [1]. It has great promise for utilizing in clean, high-efficiency power generation systems such as fuel cells.

Methanol is a good hydrogen resource because of its high hydrogen/carbon ratio. Significant efforts have been made for photo-induced reforming of methanol. The idea is to use an efficient photocatalyst together with solar energy to promote H_2 formation from methanol according to equation (1) [2]:

$$CH_3OH + H_2O \xrightleftharpoons{\text{Photocatalyst, h}\nu} 3\,H_2 + CO_2 \qquad (1)$$

Ga-oxynitride [3-5] and Ga-Zn-oxynitride [4] photocatalysts can be efficiently applied for utilizing visible light [6], they are good candidates for photocatalytic reforming of methanol [5,7]. Both materials are semiconductors, their band gaps are reduced [5] in comparison to GaN (~3.4 eV), ZnO (~3.2 eV) and Ga_2O_3 (~4.6 eV). Ga-oxynitrides have a chemical formula of $(Ga_{1-x}\ _x)(N,O)$ and can adopt the wurtzite-type structure of the hexagonal GaN (GaN_h), in which O substitutes for N and the octahedral sites are randomly occupied by Ga and vacancies [3]. In Ref [8-10] a range of $(Ga_{1-x}Zn_x)(N_{1-x}O_x)$ materials were synthesized; these wurtzite-type phases can be regarded as solid solutions of the two constituents GaN and ZnO, in which Ga and Zn randomly occupy the octahedral cation sites. The Ga-Zn-oxynitride ($(Ga_{1-x}Zn_x)(N,O)$) structure can be related to the GaN-ZnO solid solution structure by incorporation of more O to the N sites and compensating vacancies to the cationic sites, resulting in an imperfect wurtzite-type material.

Ga-oxynitrides, Ga-Zn-oxynitrides and GaN-ZnO solid solutions, which are isostructural with GaN_h, are commonly synthesized via high temperature ammonolysis of the appropriate oxide [8-10] or hydroxide precursors [4,5]. However, many parameters of the preparations, among others temperature and duration of the ammonolysis, geometry of the reactor, the gas flow and even the pre-calcination of the precursor ZnO [8], can significantly influence the properties, thus the activity of the photocatalysts. In particular, the degree of the crystallinity in Ga-Zn-oxynitrides increases with increasing nitridation time and in parallel the Zn and O concentration decreases because the significant part of the ZnO precursor is removed as a result of reduction and volatilization of the Zn [9]. The decrease of nitridation temperature, as a method of controlling ZnO concentration, results in Ga-Zn-oxynitrides with poor crystallinity, phase separation and mixed surface oxide formation leading to poor

photocatalytic activity [11]. Literature data suggests that $Ga(OH)_3$ behaves as a more suitable precursor for Ga-oxynitride synthesis than Ga_2O_3 because its crystal lattice contains unoccupied 12-coordinate sites, which facilitate the ionic transport during the nitridation [5]. The abundance of vacancies at the octahedral sites in Ga-oxynitrides can be reduced by increasing the nitridation temperatures in the range of 750-850^oC [3] and the vacancies can be eliminated by introducing Zn^{2+} into the structure, during which a complete solid solution of $(Ga_{1-x}Zn_x)(N_{1-x}O_x)$ forms [4].

The photocatalytic activity of the semiconductors can be significantly improved by applying co-catalysts [12-15]. The H_2 formation in the methanol photocatalytic reforming reaction increases several orders of magnitude if co-catalysts have been introduced onto the surface of the semiconductor [16-18]. In the absence of co-catalysts, semiconductors induce poor H_2 evolution even in the presence of any sacrificial electron donor [13]. Co-catalysts promote the charge separation and suppress the recombination of the photogenerated electron-hole pair [13-14]. Another less emphasized but important role of the co-catalyst is to provide reaction sites for elementary reaction steps subsequent to light absorption, such as formation of molecular hydrogen and its desorption from the surface. If the surface reaction is too slow to consume the charges, the probability of charge recombination increases [13].

Noble metals such as Ag, Au, Pt and oxides such as RuO, NiO_x are considered to be effective co-catalyst. Regarding the photocatalytic hydrogen production, Pt with the largest work function is not only the best co-catalyst for electron trapping but it shows excellent catalytic activity for H^+ reduction and promotes the combination of surface hydrogen atoms into molecular H_2 as well [13]. According to literature data, Pt has the lowest activation energy for H_2 evolution [19]. In addition, Pt not only drains electrons from the semiconductor but transfers them to the solution, while other metals such as Au, Ag and Cu store the excess electrons on the metal surface due to the Helmholtz capacitance of the metal–solution interface, rather than transport electrons directly to the solvent [20,21]. Consequently, Pt is considered as the most suitable hydrogen evolution co-catalyst because of its excellent electronic and catalytic properties [13].

In order to load co-catalysts on the surface of the semiconductors several methods are available. Commonly used techniques include *in situ* photodeposition [5,12,22] and deposition of pre-prepared metal colloids [23-26]. An easy and effective way for preparing co-catalysts is impregnation with the appropriate metal salt followed by calcination. A series of metal oxide co-catalysts (such as NiO_x, RuO_2, RhO_x, and PtO_x) can be built on the surface of Ga-Zn-oxynitrides by means of this method [27]. RuO_2 can also be loaded via

impregnation by tetrahydrofuran solution of $Ru_3(CO)_{12}$ followed by drying and calcination [9]. Calcination of the Ga-Zn-oxynitride support itself is preferred because the treatment eliminates the traces of metallic Zn, which are potential recombination centers [28]. According to [29,30], the Rh_x-Cr_y-oxide pair, obtained by co-impregnation (co-evaporation) followed by calcination, is one of the most effective co-catalysts in the overall water splitting on Ga-Zn-oxynitrides. However, this co-catalysts/semiconductor system is less effective in the methanol photocatalytic reforming reaction [31]. High temperature reduction of the metal precursor [32] in H_2 is one of the most commonly used methods to prepare supported metal catalysts, but it is believed unsuitable for oxynitrides because of their limited thermal stability compared to oxides [33].

In this contribution the structural stability of the Ga-Zn-oxynitride/Pt co-catalyst system is discussed. The effect of the synthesis steps on the structural properties of the catalysts is compared in case of two distinct Ga-Zn precursor compounds. The study is completed by exploring the structural evolution of the catalyst systems during the reaction conditions of photocatalytic H_2 production.

2. Materials and methods

2.1 Materials

$Ga(NO_3)_3$ (Aldrich), Ga_2O_3 (Aldrich), ZnO (Aldrich), GaN (Aldrich), $Pt(NH_3)_4(NO_3)_2$ (Aldrich), $Zn(NO_3)_2x6H_2O$ (Fluka), urea (Molar Chemicals Ltd, Hungary) were used as received. Methanol and NH_4OH solution were purchased from Reanal (Hungary). Double distilled water (18 MΩ) was used in every experiments.

2.2 Synthesis of the photocatalysts

We assumed that homogeneous distribution of the components was favorable to retain Zn during the nitridation process. Therefore a co-precipitation method starting from Ga and Zn salts was chosen to obtain the precursors for high temperature NH_3 treatment. The Zn/Ga starting (Zn/Ga_{nom}) ratio was controlled by the amount of the precursor materials. For example, in order to achieve a Zn/Ga_{nom} atomic ratio of 0.32, we dissolved 2.43 g $Ga(NO_3)_3$ and 0.89 g $Zn(NO_3)_2x6H_2O$ in 50 ml water and added 1.03 g urea. The mixture was irradiated in a microwave reactor for 30 min at 120°C. Then the mixture was stirred at 60°C as long as the NH_3 gas liberated (checked by the color change of the pH paper over the mixture). As a result a precipitate formed, which was separated by centrifugation and washed with 3x50 ml

water to remove the nitrate. The sample was dried in an oven at 90°C for overnight. The nitridation was carried out in a quartz reactor using 100 ml/min NH_3 flow at 800°C for 10h. The relatively low temperature was chosen in order to reduce the release of Zn. For comparison, the same preparation steps were performed by mixing Ga_2O_3 and ZnO starting materials with Zn/Ga_{nom} ratio of 0.32. We also synthesized samples with Zn/Ga_{nom}=0.14 from both the nitrate and oxide starting materials. The quality and behavior of the prepared samples were compared to commercial GaN.

As a co-catalyst, 1% Pt was introduced by impregnation with the aqueous solution of $Pt(NH_3)_4(NO_3)_2$. After overnight drying at 90°C, the samples were either calcined for 1h at 300°C in an oven using 1 °C/min heating rate or were reduced in 30 ml/min H_2 flow at 450°C for 1h using stepwise heating in H_2 after purge with N_2 at 150°C for 15 min.

2.3 Characterization of the photocatalysts

X-ray powder diffraction (XRD) patterns were obtained in a Philips model PW 3710 based PW 1050 Bragg-Brentano parafocusing goniometer using CuK_α radiation (λ= 0.15418 nm), graphite monochromator and proportional counter. Silicon powder (NIST SRM 640) or corundum were used as internal standards and the scans were evaluated with profile fitting methods. During phase analysis we used reference cards from the ICDD PDF-2 (1998) data base. The cell parameters of the crystalline phases were determined from the d-values of all the reflections. Crystallite sizes were calculated from reflection line broadening using the Scherrer-equation.

TEM studies of the samples were carried out in a FEI Morgagni 268D type transmission electron microscope (accelerating voltage: 100 kV, W-filament). The samples were prepared by grinding and dispersing of the resulted powder in ethanol using an ultrasonic bath. Energy Dispersive X-ray Spectrometry (EDX) analysis was performed by an INCA (Oxford Instruments Ltd.) detector and an INCA Energy software package attached to a ZEISS EVO 40XVP Scanning Electron Microscope (accelerating voltage: 20kV, W-filament, working distance 10 mm).

X-ray photoelectron spectroscopy (XPS) measurements were carried out using an EA125 electron spectrometer manufactured by OMICRON Nanotechnology GmbH (Germany). In order to overcome difficulties due to overlap of the C 1s and N 1s lines with Ga Auger transitions, the photoelectrons were excited by both MgKα (1253.6 eV) and AlKα (1486.6 eV) radiation. Spectra were recorded in the Constant Analyzer Energy mode of the energy analyzer with 30 eV pass energy resulting in a spectral resolution around 1 eV.

Samples in the form of fine powder were pressed into pellets. Binding energies were referenced to the hydrocarbon component of the C 1s peak arising from adventitious contamination at 285.0 eV. Since compositional analysis suggested a strongly oxidized/hydroxilated state for the surface, a secondary reference was the Ga $2p_{3/2}$ peak, which was expected around 1118.8 eV in Ga_2O_3 [34]. Data were processed using the CasaXPS software package [35] by fitting the spectra with Gaussian-Lorentzian product peaks after removing a Shirley or linear background. Nominal surface compositions were calculated using the XPS MultiQuant software package [36,37] with the assumption of homogeneous depth distribution for all components. Chemical states were identified by XPS databases [38,39].

2.4 Photocatalytic hydrogen generation

The photocatalytic reforming reaction of methanol was carried out in an UV-Consultig Peschl UV-Reactor System 1 equipped with gas inputs and outputs. We monitored the reactions at least for a day. N_2 with 20 ml/min flow rate was continuously bubbled through the reactor. The gas outlet was connected to a gas chromatograph (Agilent 7820A, SUPELCO Carboxen 1010 column, TCD and FID detections and argon internal standard) to follow H_2 formation. Initial concentration of methanol was 6 vol% in double distilled water. Literature reports suggested that the rate of hydrogen generation *vs*. methanol concentration had a saturation curve and therefore the use of diluted solution was favorable [40]. The photocatalytic reaction was carried out at 30-35^{o}C. The amount of catalyst and the reaction volume were 50-300 mg and 370 ml, respectively. A mercury medium pressure lamp TQ 150 Z2 (150 W) operating in UV-visible region was used as light source. After the photocatalytic reaction, the samples were recovered from the aqueous methanol solution by centrifuging, washing with 3x50 ml absolute ethanol followed by drying under N_2 flow.

3. Results and discussion

3.1 Characterization of oxynitrides

All of the samples recovered after high temperature nitridation, obtained either from the precipitates or from the oxide mixtures, had a color of dark yellow to orange. Their corresponding XRD patterns exhibited exclusively the characteristic lines of the hexagonal wurtzite-type structure (see Figure 1) similar to GaN (# 76-0703) and ZnO (zincite) (# 36-1451). None of the prepared oxynitride samples contained crystalline Ga_2O_3 (# 87-1901) or

cubic ZnO. We interpreted the elevated background as resulting from a small amount of an amorphous phase. The average crystallite sizes were 14-15 nm for the samples recovered from precipitates and 38-40 nm for those obtained from oxides.

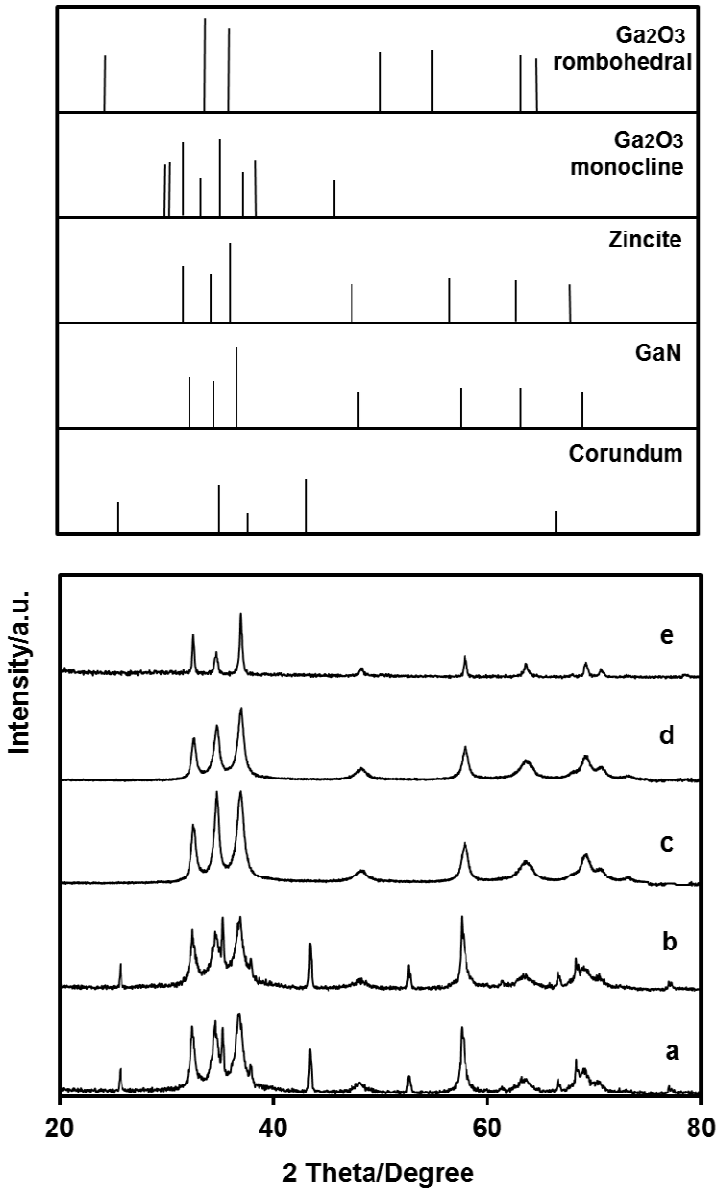

Figure 1. XRD patterns of the Ga-Zn-oxynitrides obtained by nitridation of different precursors. a= sample obtained by nitridation of the precipitate from $Zn(NO_3)_2$ and $Ga(NO_3)_3$ with Zn/Ga_{nom}=0.32 (corundum internal standard added); b= sample obtained by nitridation of the precipitate from $Zn(NO_3)_2$ and $Ga(NO_3)_3$ with Zn/Ga_{nom}=0.14 (corundum internal standard added); c= sample obtained by nitridation of oxide mixture with Zn/Ga_{nom}=0.32; d= sample obtained by nitridation of oxide mixture with Zn/Ga_{nom}=0.14; e= GaN (commercial)

As a result of Zn incorporation into the oxynitride, the positions of the diffraction peaks were slightly shifted to lower 2Θ angles than those of GaN (see details in the Supplementary material, section S1). Nitridation of both precipitates and oxide mixture resulted in oxynitrides similar to those described by Miyaake and coworkers [4]. The lattice parameters depicted in Figure 5 of Ref. [4] (a=3.194 Å, c=5.214 Å at Zn/Ga=0.11) were in accordance with our results (a=3.195Å, c=5.182Å at Zn/Ga_{EDX}=0.11).

TEM images of nitridated samples of Ga-Zn-oxynitrides (Figure 2A, B) showed nanocrystals. Nitridation of the precipitate from Zn- and Ga-nitrate solution resulted in 20-40 nm rounded crystals, whereas the crystallites were larger (40-200 nm) for the sample obtained by nitridation of the oxide. Moreover, these crystals were aggregated into 1 μm wide and 5 μm long rods preserving the morphology of the parent Ga_2O_3. In contrast, the commercial GaN (Figure 2C) consisted of very large (micrometer) crystals. The electron diffraction patterns of each sample were indexed according to the hexagonal wurtzite (# 76-0703) consistently with XRD result.

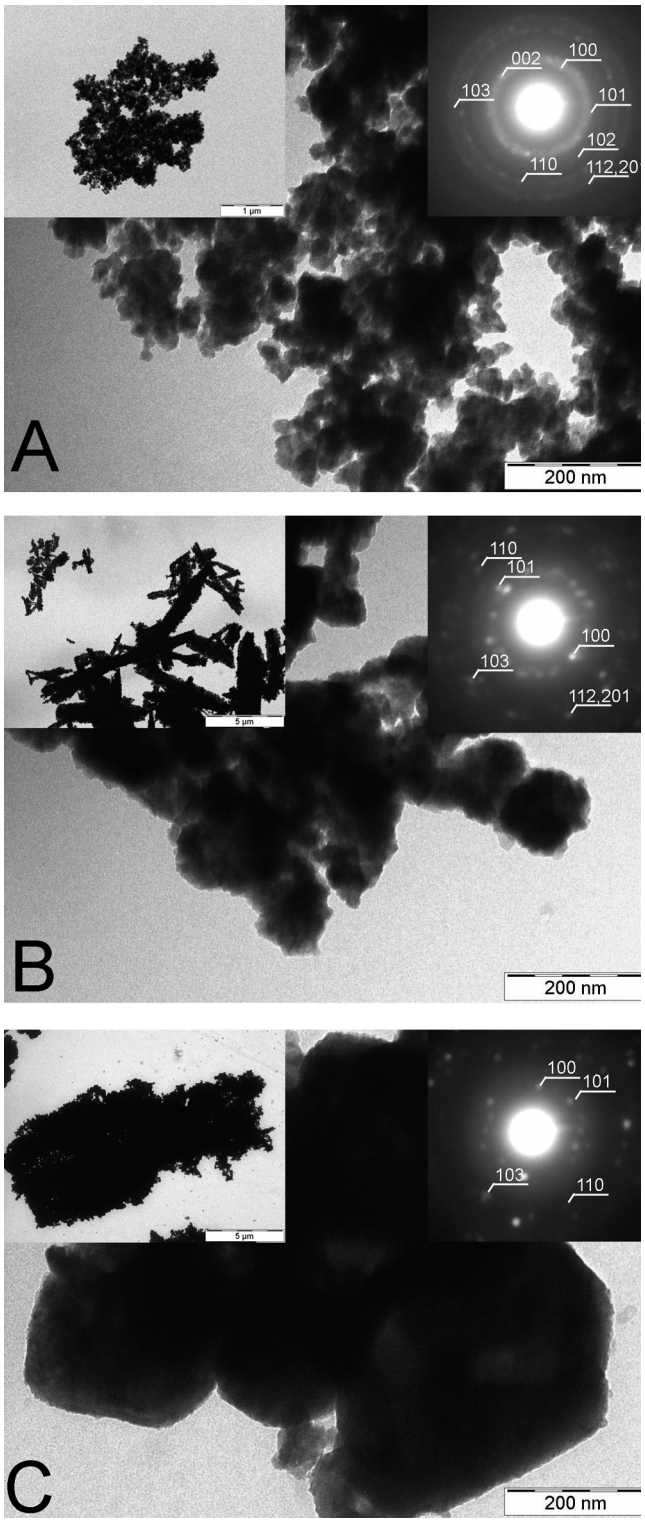

Figure 2. TEM images of the Ga-Zn-oxynitrides obtained by nitridation of different precursors (Zn/Ga_{nom}=0.32). A: nitridation of the precipitate from Zn- and Ga- nitrate solution; B: nitridation of oxide mixture; C: commercial GaN. Electron diffraction patterns (inserts) reveal the presence of hexagonal wurtzite (# 76-0703).

The surface concentrations and chemical states of the elements of the Ga-Zn-oxynitride samples prepared by different methods were determined by XPS measurements. The Ga content was estimated using the intensity of the Ga 3d band. The results were compared to those obtained on commercial Ga_2O_3 and GaN references. In Table 1 characteristic binding energies, N/Ga and Zn/Ga ratios were summarized for representative examples of the prepared photocatalysts. In case of the Ga_2O_3 reference the relatively narrow Ga 3d peak was found at 20.5 eV, a value consistent with the nominal fully oxidized state (Ga_2O_3) [34,38,39]. The 1062.2 eV kinetic energy for the Ga $L_3M_{45}M_{45}$ Auger transition was also in the range reported for Ga_2O_3 (1062-1063 eV). The Auger parameter calculated as the sum of the binding energy of the Ga 3d band and the kinetic energy of the Ga $L_3M_{45}M_{45}$ Auger peak was at 1082.7 eV, which is also in good agreement with data available for Ga_2O_3.

The binding energy reported for the Ga 3d peak of GaN was around 19.5-20.0 eV [41-46]. The value observed in the present study for the reference GaN was at the upper limit (20.0 eV) of this range. On the other hand, according to quantitative analysis, the surface was rather nitrogen-deficient and contained a high amount of oxygen. At the same time, the N 1s binding energy of 398.4 eV was well above the values reported in the literature for GaN (397.2-397.5 eV [9,41-43,45,46]), which could be interpreted in terms of formation of a heavily oxidized surface layer, in which the local environment of the N atoms was quite different from that in GaN. Indeed, literature reports for similarly high N 1s binding energies suggested the occurrence of oxygen-exposed GaN surfaces [42,47]. This mixed nature also influenced the Ga Auger parameter, which was at 1083.5 eV, an intermediate value between those characteristic for Ga_2O_3 (1082.7 eV) and GaN (1084.1 eV) [46].

Structural studies revealed that both classes of the GaN-ZnO photocatalysts (i.e. the ones made from precipitates or from oxides) could be regarded as Ga-Zn-oxynitrides. As far as their XPS characteristics were concerned, they were rather close to each other. The 20.1-20.2 eV binding energy for the Ga 3d band, the Ga Auger parameter somewhat above 1083 eV and the strong N deficiency were all in very good agreement with the mixed, oxygen- and nitrogen-containing local environment for Ga, as expected for oxynitrides. Indeed, in Ref. [42] a Ga 3d contribution at 20.2 eV was observed on an oxidized GaN sample and was attributed to Ga-oxynitride. The Zn content, which was considerable for the material prepared from precipitates but was very small for the oxide derived samples, was in its fully oxidized state as based on the Zn $2p_{3/2}$ binding energy (somewhat above 1022 eV) and the Zn $L_3M_{45}M_{45}$ kinetic energy (around 989.0 eV) [38,39].

In all studied samples the O 1s peak was separated into two contributions; the binding energy of the stronger one corresponded to the range reported for Ga_2O_3 (530.7-531.3 eV) suggesting again that the nitridation remained incomplete. The weaker contribution around 532.3-532.8 eV was also observed in GaN and could be assigned to surface oxygen containing species like OH groups [9].

In Table 2 we summarized the nominal Zn/Ga_{nom} ratio and the experimental Zn/Ga ratios derived from XPS (Zn/Ga_{XPS}) and EDX (Zn/Ga_{EDX}) measurements of the nitrided samples. The Zn/Ga_{EDX} was lower than the Zn/Ga_{nom} for all samples. The Zn deficiency was particularly striking in the samples obtained from oxide mixtures, as also suggested by the XPS data. It was obvious that some part of the Zn was removed during the preparation, *i.e.* it was washed out and/or it was volatilized during the nitridation [9] despite the relatively low temperature of the NH_3 treatment. The latter was much likely affected by the Zn content. The Zn retention during the nitridation was larger in the samples obtained from precipitates than those from oxides (cf. Zn/Ga_{nom} and Zn/Ga_{EDX} values in Table 2). This observation could be explained by the better distribution of the components in the precursor of the nitridation, which was similar to the gel-formation method used by Ward and coworkers [11]. The parallel experiments showed acceptable reproducibility of the preparation of the Zn-Ga-oxynitrides.

The optical properties of the studied Ga-Zn-oxynitrides were investigated by diffuse reflectance UV-visible spectrophotometry. The results are summarized in the Supplementary Material (section S2). The band gap values derived from the UV-visible spectra were in agreement with those available in the literature [9, 31].

3.2 Loading of the Pt co-catalyst

As it was mentioned above, adequate activity in the photocatalytic hydrogen production could not be achieved without a metallic co-catalyst like Pt [13,18,27]. One of our main questions was whether the hydrogenation and the calcination processes, which were necessary for the formation of the co-catalyst from the impregnated precursor salt on the surface of the oxynitride, would change the semiconductor.

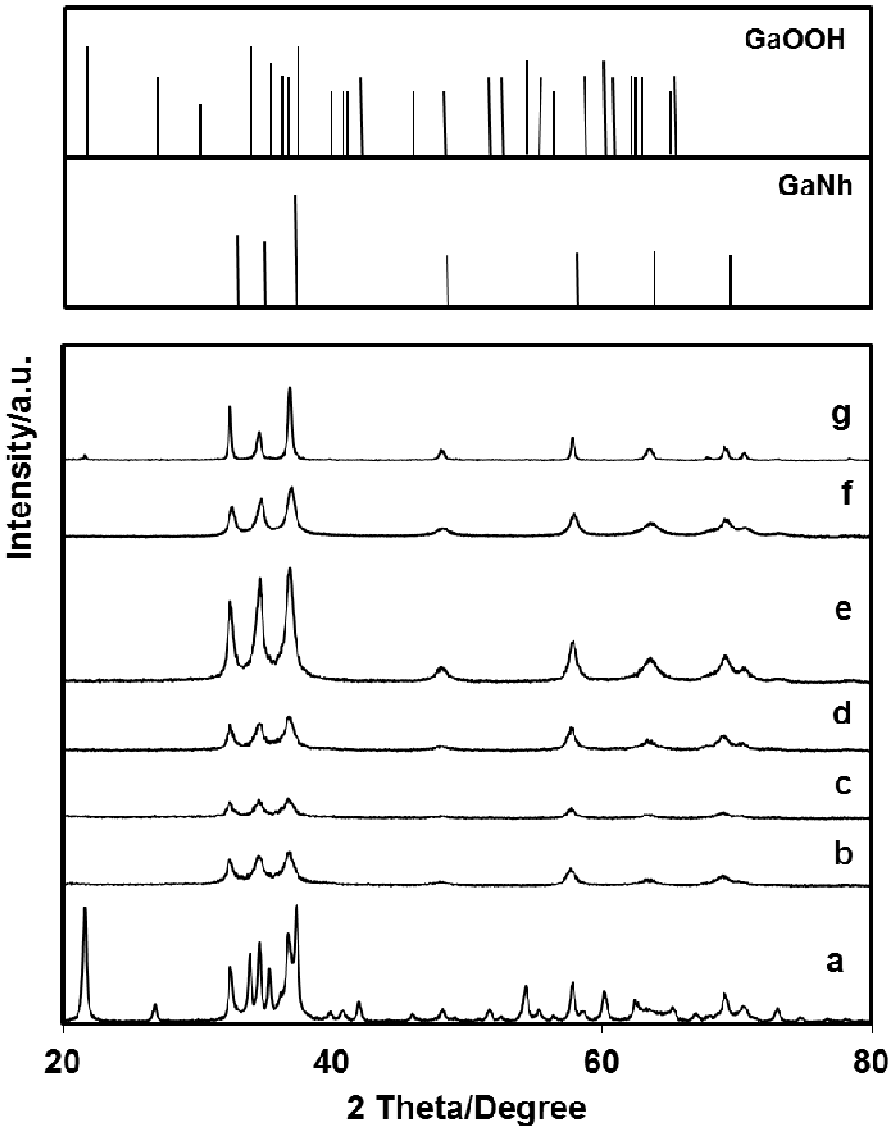

Figure 3. XRD patterns of the Pt loaded Ga-Zn-oxynitrides after different treatments of the Pt precursor.

a= nitrided precipitate, Pt formation by calcination; b= nitrided precipitate, calcination after "blank" impregnation (impregnation with no Pt precursor in the solution); c= nitrided precipitate, calcination without impregnation; d= nitrided precipitate, Pt formation by hydrogenation; e= nitrided oxides, Pt formation by calcination; f= nitrided oxides, Pt formation by hydrogenation g= GaN (commercial), Pt formation by calcination.

Zn/Ga_{nom}: a-d=0.32, e-f=0.14, Pt load (when applicable) = 1%.

According to our experiments, the post-treatment process could significantly influence the XRD patterns of the Ga-Zn-oxynitrides (Figure 3). It could be seen that the hexagonal wurtzite-type structure was maintained if the Pt precursor was reduced in H_2 at 450^{o}C (see

lines d, f in Figure 3). The XRD results also revealed that the H_2 treatment of the unloaded oxynitride itself at 450°C did not change the structure (not shown). Similarly, the calcination process itself did not change the bulk oxynitride structure (see line c in Figure 3). However, the XRD pattern changed drastically if the Pt precursor was calcined in air (see line a in Figure 3). Beside the wurtzite-type structure, significant amount of a new phase appeared, which could be identified as α-GaOOH (# 87-1901) [48,49]. It was described that deuterated GaOOD formed under hydrothermal conditions and remained stable up to 300°C [48]. Other study reported that flower-like α-GaOOH formed at 175°C, which converted to a rodlike α-Ga_2O_3 after calcination at 450 °C [49]. Our experiments suggested that Pt played a decisive role in the phase transition of the oxynitride. Additionally we could propose the occurrence of a Zn-containing Ga-oxyhydroxide (Ga(Zn)-oxyhydroxide) phase for Zn incorporation into oxyhydroxides in analogy to the oxynitrides. Furthermore, no phase transition was observed in a "blank impregnation" without platinum salt (line b in Figure 3) supporting the preliminary importance of Pt in the process.

N_2 purge at 150°C, used before the H_2 reduction, removed the water, which probably also contributed to the lack of the appearance of oxyhydroxide during the co-catalyst formation by hydrogenation. Thus, we concluded that water in the atmosphere used in calcination had an important role in the transformation of the oxynitride into oxyhydroxide, during which nitrogen and excess hydrogen might be released in molecular form.

According to XRD results, the oxyhydroxide phase did not appear during the formation of the co-catalyst by calcination for samples obtained from the oxides (see line e in Figure 3). The lack of the oxyhydroxide phase could be explained by the significantly larger grain size and smaller surface area, in contrast to those prepared via precipitation. The oxyhydroxide formation in the presence of Pt likely started from the surface of the nanoparticles. The commercial GaN also maintained its wurtzite structure and did not show the presence of oxyhydroxide if GaN was calcined after impregnation with the Pt precursor (see line f in Figure 3).

TEM images of the Pt/Ga-Zn-oxynitride samples (Figure 4) supported the XRD results. Pt co-catalyst formation via hydrogenation of samples obtained from either precipitate or oxide mixture did not change the morphology and the grain size in respect to the parent oxynitride (cf. Figure 2A-Figure 4A and Figure 2B-Figure 4B). As expected from the XRD data, co-catalyst formation via calcination of samples obtained from oxide mixture also preserved the morphology (cf. Figure 2B-Figure 4D). However, calcination of the Pt-loaded samples obtained from precipitates resulted in a drastic change of the morphology: the

originally more or less globular grains coalesced into large rod-like features (Figure 4C), suggesting large-scale material transport accompanied by the appearance of the oxyhydroxide phase.

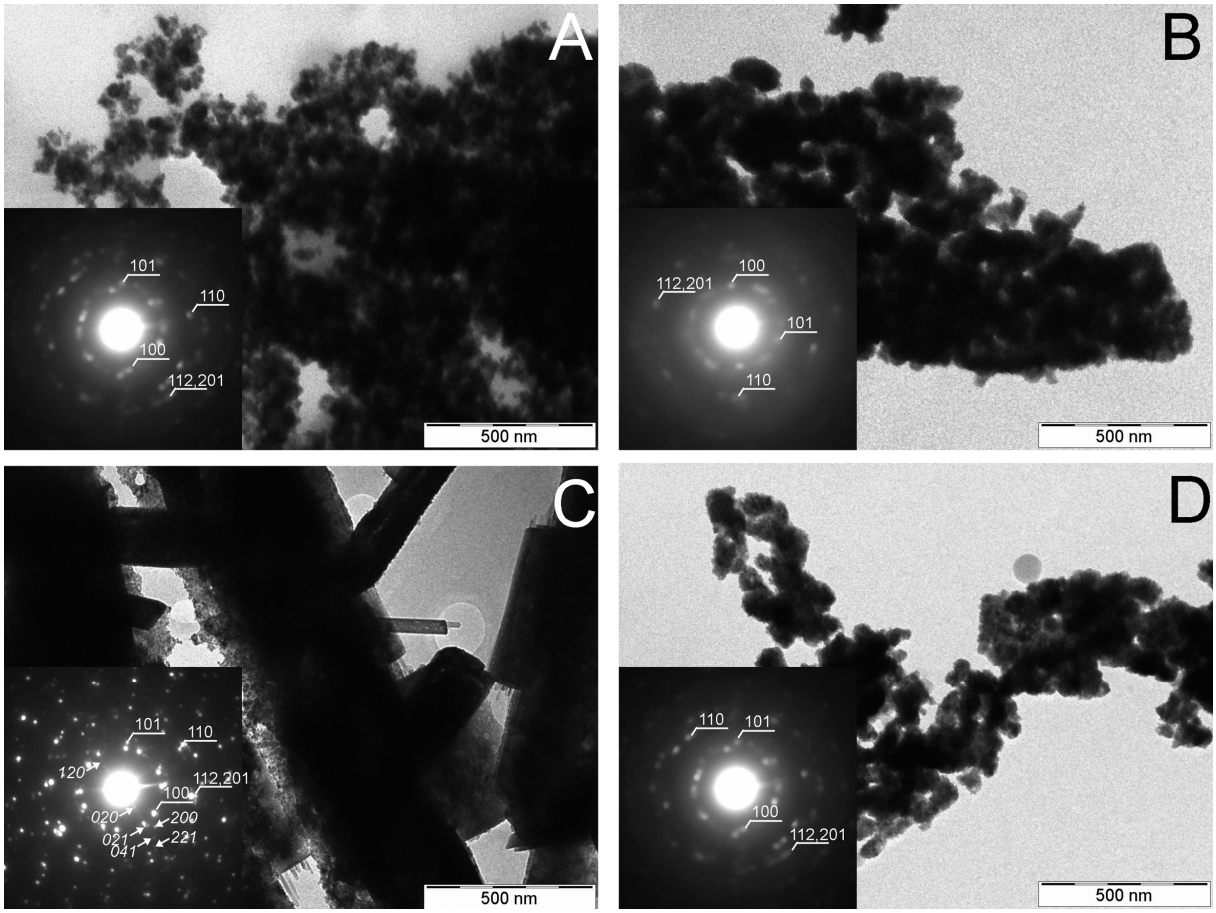

Figure 4. TEM images of the Pt/Ga-Zn-oxynitrides (Zn/Ga_{nom}=0.32) obtained by different formation of Pt co-catalyst. A: sample from precipitate, Pt co-catalyst formed by hydrogenation at 450^{o}C; B: sample from oxide mixture, Pt co-catalyst formed by hydrogenation at 450^{o}C; C: sample from precipitate, Pt co-catalyst formed by calcination at 300^{o}C; D: sample from oxide, Pt co-catalyst formed by calcination at 300^{o}C. Consistently with XRD result, electron diffraction patterns (inserts) revealed the presence of hexagonal wurtzite (# 76-0703) and for C GaOOH diffractions (# 87-1901), which are indicated by arrows.

The XPS characteristics of selected reduced or calcined Ga-Zn-oxynitrides (Supplementary Material section S2, Table S2) were essentially undistinguishable from those

of the as synthesized materials, confirming that neither reduction nor calcination altered even the surface of the photocatalysts if they were free of Pt.

In Table 3 XPS data demonstrating the response of the Pt-loaded Ga-Zn-oxynitrides to the reductive treatment and the calcination were shown. In order to visualize some tendencies in the data, in Figure S3.1 of the Supplementary material Ga 3d spectra at different stages of the life cycle of the oxide derived sample with $Zn/Ga_{nom}=0.32$ were summarized. In Figure S3.2 the change of the Ga Auger parameter for the same sample was given from the as prepared state up to the recovered state after the photocatalytic reaction.

The Ga 3d binding energies (Table 3) were essentially identical for all Pt-loaded samples (slightly above 20 eV). On the contrary, the Ga Auger parameters and the N/Ga ratios revealed significant changes for the calcined Pt/ Ga-Zn-oxynitrides, regardless if they were derived from precipitates or oxides. The shift of the Auger parameter towards lower values upon Pt loading (see also Figure S3.2, Supplementary Material) was consistent with a more oxidized local environment for Ga and the strongly decreasing N content also pointed to the growth of an oxidized phase during calcination, which, according to the XRD and TEM data of the calcined Pt/ Ga-Zn samples obtained from precipitates (Figure 3, Figure 4C), could be identified as Ga- or Ga(Zn)-oxyhydroxide. As the Zn content was hardly influenced by the treatments, the latter identification seemed to be more probable. According to literature data, the reported Ga 3d binding energy for Ga-oxyhydroxide species on water-exposed GaAs was 20.0-20.2 eV [50]. Thus, the Ga 3d binding energies of Ga-oxynitride and the Ga-oxyhydroxide phases were indistinctive; for their identification the Ga Auger parameter was also necessary.

XRD and TEM investigations suggested that the oxynitride to oxyhydroxide transition occurred in the presence of Pt and water under oxidative conditions. Data of Table 3 confirmed these results, as only the reduced Pt/Ga-Zn-oxynitride sample prepared from precipitates retained its oxynitride characteristics. In addition, while bulk-sensitive structural methods revealed no changes for the oxide-derived calcined Pt/Ga-Zn-oxynitride sample, the surface sensitive XPS clearly demonstrated its oxidized nature (Figures S3.1 and S3.2 in the Supplementary Material), indicating that the transformation should have been initiated on the surface of the particles. Nevertheless, the initial structure of the semiconductor particles had an important role during the transition. While the Pt-containing oxynitrides seemed to be unstable, the surface of the Pt-loaded commercial GaN sample consisting of large and compact semiconductor grains remained essentially unchanged upon calcination, even if the

shift of the N 1s peak towards lower binding energies might indicate an initial structural rearrangement.

XPS also provided information on the state of Pt, which was difficult to assess by XRD or TEM due to the very small loading. The influence of the treatments on the Pt 4f spectra was depicted in Figure 5.

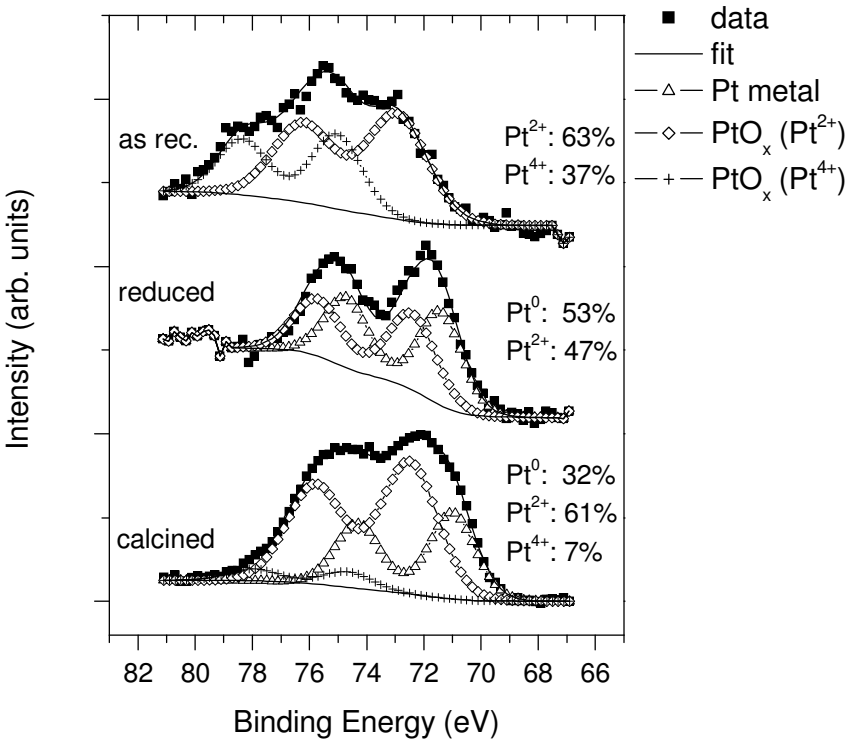

Figure 5. Pt 4f spectra of an impregnated, a hydrogen treated and a calcined Pt/Ga-Zn-oxynitride sample obtained from nitridation of the precipitate. Zn/Ga_{nom}=0.14; Pt content= 1 w%.

In the impregnated sample initially two almost equal Pt $4f_{7/2}$ contributions were identified, one at 72.8 eV and the other at 74.9 eV. According to the literature, a Pt $4f_{7/2}$ peak around 72.5 eV occurred as the results of Pt^{2+} ions (e.g. $Pt(OH)_2$), whereas Pt $4f_{7/2}$ binding energies around 74-75 eV were characteristic for Pt^{4+} (like PtO_2) [51,52]. A gradual reduction of Pt was observed in the course of the XPS measurement (Table 3, not shown in Figure 5), as evidenced by the decrease of the Pt^{4+} contribution and the appearance of the metallic Pt signal

around 71 eV. In the Pt 4f spectra of the calcined samples, the Pt^{2+} ionic state gave the dominating contribution, whereas a smaller metallic signal was always present. On the other hand, reductive treatment resulted in almost equal Pt^{2+} and metallic Pt contributions. A similar response to calcination and reduction was commonly reported for oxide supported Pt catalysts [53]. The amount of Pt corresponded well to the intended 1 m/m% in all samples. The transformation of the oxynitride material seemed not connected to the oxidation level of Pt, as qualitatively similar Pt 4f spectra were obtained from non-transformed and heavily transformed samples. Nevertheless, Pt $4f_{7/2}$ binding energies of Table 3 suggested that the metallic contribution shifted towards lower values, below 71 eV, if the surface became hydroxylated.

3.3 The influence of the photocatalytic H_2 production on the photocatalysts

Both Pt/Ga-Zn-oxynitride samples obtained from either oxide mixtures or precipitates showed higher H_2 production than the Pt/GaN samples (Figure 6). Similar H_2 productions for Pt/Ga-Zn-oxynitride pairs from oxide mixtures and precipitates were observed. We found that co-catalyst formation obtained by calcination resulted in better performance for each samples than those obtained by hydrogen treatment (cf. dotted and striped columns).

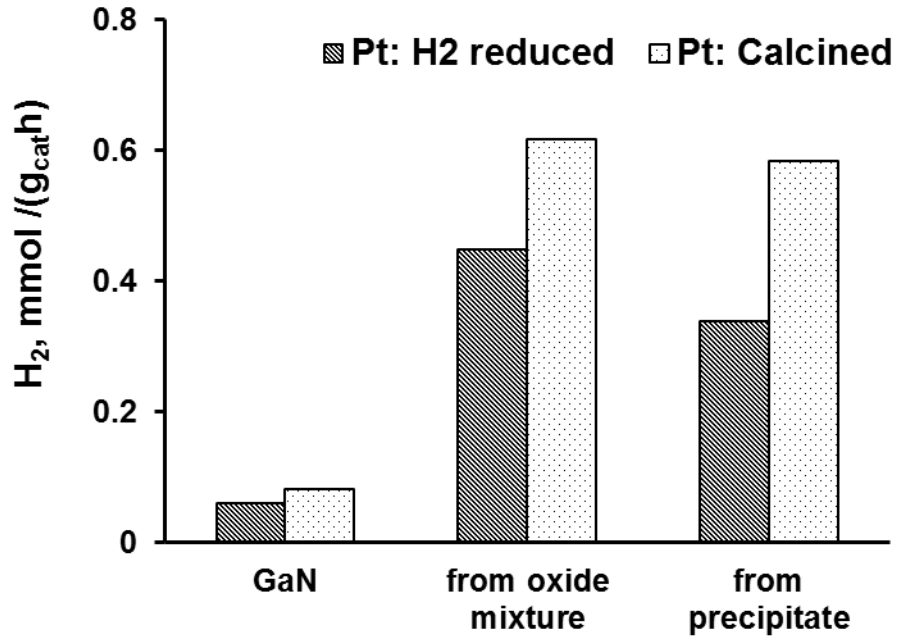

Figure 6. Photocatalytic hydrogen production over Pt/Ga-Zn-oxynitride catalysts obtained by different preparation methods. Zn/Ga_{nom}=0.32, Pt content= 1 w%; T= 30-35 ^oC, t= 4 h (steady state);
Pt: H2 reduced - formation of Pt co-catalyst by H_2 treatment at 450^oC;
Pt: Calcined - formation of Pt co-catalyst by calcination at 300^oC;
from oxide mixture: obtained by nitridation of oxide mixture;
from precipitate: obtained by nitridation of the precipitate.

The beneficial effect of the calcination for the photocatalytic activity could be partly attributed to the removal of the traces of metal Zn. Literature data reported that Zn recombination centers could be eliminated by calcining the GaN-ZnO solid solution [28]. On the other hand, as described above, calcination in the presence of Pt strongly influenced the structure of Ga-Zn-oxynitride by enhancing the oxidation/hydroxylation of the surface. It has been described that GaN@Ga_2O_3 core-shell nanoparticles prepared by annealing of GaN nanoparticles in air showed improved photocatalytic activity during the oxidation of an azo-dye solution [54]. In addition, high-resolution XPS measurements indicated that a transitional Ga-Zn-oxynitride layer forms on the surface of GaN-ZnO solid solution photocatalysts, which was covered by a thin GaO_x outermost surface layer [55]. Thus, it might be assumed that the enhanced surface oxidation level of the Ga-Zn-oxynitride was beneficial for the photocatalytic process.

The hydrogen evolution rate was almost the same for the two types of calcined Pt/Ga-Zn photocatalysts, in spite of the fact that prior to the photocatalytic experiment the sample obtained from oxides preserved the Ga-Zn-oxynitride phase in its bulk, whereas the catalyst obtained from precipitates resulted in a new Ga(Zn)-oxyhydroxide phase (line a in Figure 3 and Figure 4C). In order to get a better understanding of the similar photocatalytic behavior of the samples having different bulk structures, we investigated the recovered samples after photocatalytic reactions using EDX, XRD, TEM and XPS methods.

The Zn/Ga_{EDX} ratio of the used catalysts decreased with 10-25 % compared to the parent oxynitrides, indicating Zn release during the catalytic reaction. The XRD results showed dramatic changes, i.e., presence of oxyhydroxide was evidenced in all samples (see line a,b,d,e in Figure 7). In addition, some wurtzite phase was detected in samples obtained from precipitates (see lines a,b in Figure 7). However, the apparent peak broadening and overlap hindered the detailed characterization of this remnant wurtzite phase.

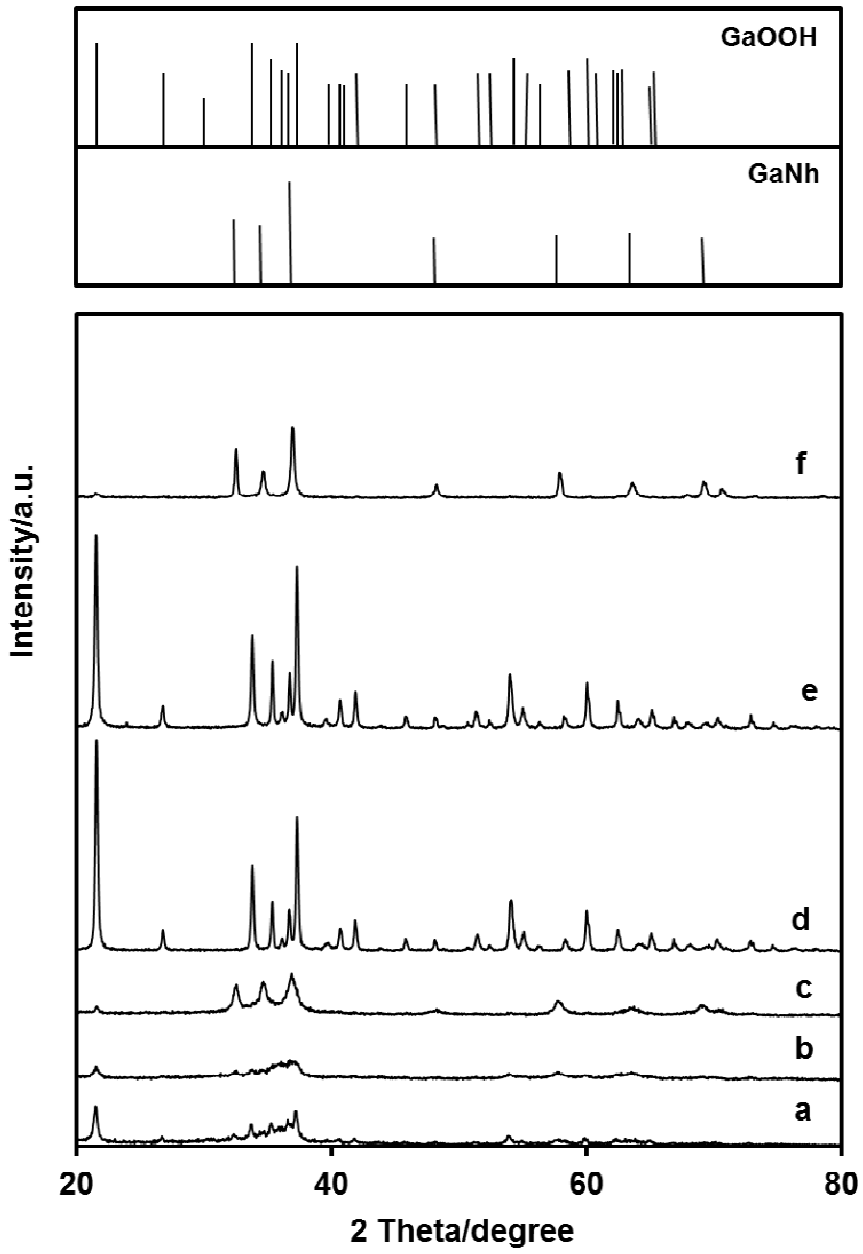

Figure 7. XRD pattern of recovered catalysts after the photocatalytic H_2 production (reaction conditions in Figure 5)

a=sample obtained from precipitate, co-catalyst formation by calcination; b= sample obtained from precipitate, co-catalyst formation by hydrogenation, c= sample obtained from precipitate, co-catalyst formation by hydrogenation, blank experiment, d= sample obtained from oxides, co-catalyst formation by calcination; e= sample obtained from oxides, co-catalyst formation by hydrogenation;

f= GaN (commercial), co-catalyst formation by calcination, blank experiment.

The TEM images of the used samples recovered after the photocatalytic H_2 production (Figure 8) confirmed the occurrence of elongated oxyhydroxide crystals, which were similar to those of the calcined Pt/ Ga-Zn sample obtained from precipitates (Figure 4C). However, the images showed the crystal size of Ga(Zn)-oxyhydroxide was larger in samples obtained from oxide mixture (500 nm wide and couple of microns long) than those from precipitate (10-100 nm wide and 500-1000 nm long). ED indicated remnant wurtzite Ga-Zn-oxynitride in one of the samples obtained from precipitate (Figure 8C).

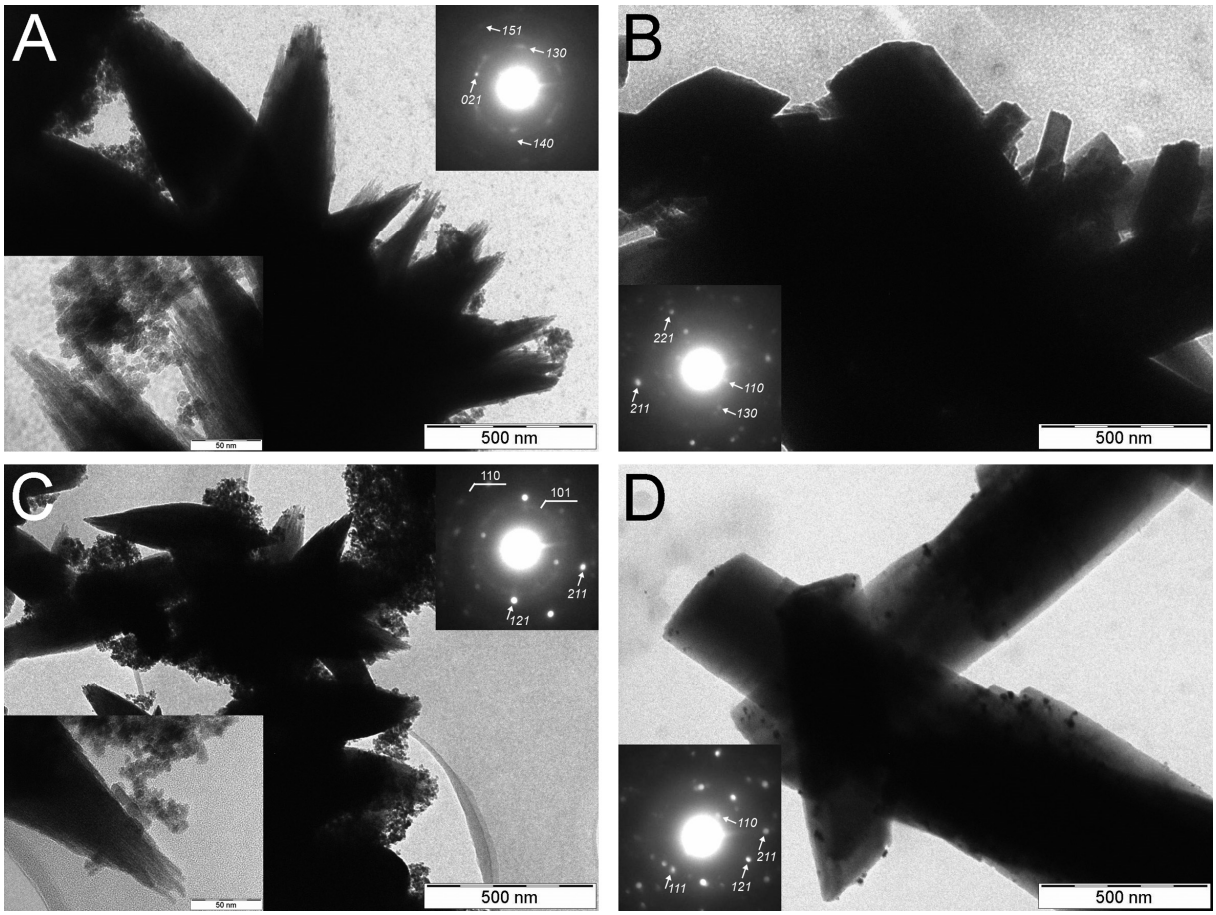

Figure 8. TEM images of the Pt/Ga-Zn-oxynitride photocatalysts recovered after the photocatalytic H_2 production (reaction conditions in Figure 5). A: used catalyst from precipitate, Pt co-catalyst formed by hydrogenation at 450^{o}C; B: used catalyst from oxide mixture, Pt co-catalyst formed by hydrogenation at 450^{o}C; C: used catalyst from precipitate, Pt co-catalyst formed by calcination at 300^{o}C; D: used catalyst from oxide, Pt co-catalyst formed by calcination at 300^{o}C. Consistently with XRD result, arrows in electron diffraction patterns (inserts) point to GaOOH diffractions (# 87-1901). 101 and 110 indices in C indicate hexagonal wurtzite (# 76-0703) contributions.

In order to get some insight into the influence of the photocatalytic reaction on the oxynitride to oxyhydroxide phase transition, we performed blank experiments, i.e., we stirred selected catalysts in methanol solution without irradiation. The XRD measurement showed that both the Pt/GaN (co-catalysts formed by calcination) and the Pt/Zn-Ga-oxynitride obtained from precipitate (co-catalysts formed by hydrogenation) mainly maintained the wurtzite structure (see line c, f in Figure 7). Although one of the most intensive reflections of the GaOOH (at 2Θ~22^{o}) was observed in the blank samples, these blank experiments indicated irradiation and/or in-situ hydrogen formation had a key role for the oxynitride to oxyhydroxide phase transition of the working photocatalysts.

In order to show how the transformation of the bulk of the used Pt/Ga-Zn-oxynitride photocatalysts influenced the surface properties, we compared the XPS characteristics of the used catalysts and those measured on the blank used calcined Pt-GaN sample (Table 4). As far as the chemical states of Ga, Zn and O were concerned, each of the four samples recovered from the photocatalytic reaction were very similar to each other. As it was pointed out in connection with the reduced/calcined Pt-loaded photocatalysts, the Ga 3d binding energy slightly above 20 eV might indicate the presence of either Ga-oxynitrides or Ga- or Ga(Zn)-oxyhydroxides; accordingly, there was no notable shift in the example given in Figure S3.1 of the Supplementary Material. The Ga Auger parameter confirmed a strongly oxidized environment for Ga in all used photocatalysts (see also Figure S3.2 of the Supplementary Material), with the exception of the (not irradiated) Pt/GaN system, in which the oxynitride-like Ga environment was still preserved (Table 4, entry 2).

In the O 1s spectrum of the used Pt/Ga-Zn-oxynitride photocatalysts a pronounced component around 532.5 eV indicated the presence of hydroxyl species, confirming the formation of oxyhydroxides. As a representative example, Figure 9 depicted the O 1s core level spectra of a Pt-loaded, reduced sample derived from precipitates before and after the photocatalytic experiment. In parallel with the surface transformation, a very significant loss of N was evident. Thus, in good agreement with the structural studies, XPS also confirmed the (almost complete) transformation of the Pt/Ga-Zn-oxynitride photocatalysts into Pt/Ga(Zn)-oxyhydroxides during the photocatalytic reaction.

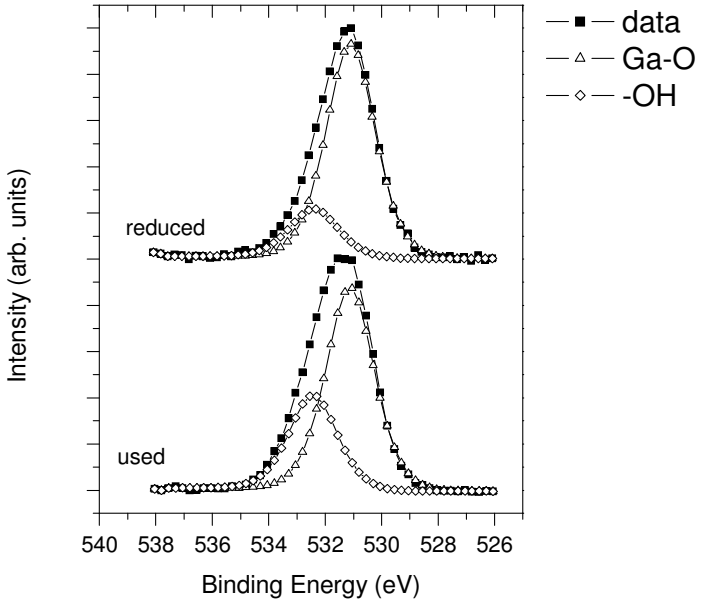

Figure 9. O 1s spectra of the reduced and used Pt/GaN-ZnO photocatalysts derived from precipitates (Zn/Ga_{nom}=0.32). Top line: reduced, before the photocatalytic reaction; bottom spectrum: the same sample recovered after the photocatalytic reaction

The surface Zn content remained relatively abundant in the samples obtained by precipitation (compare data in Table 1 and 4); the Zn $2p_{3/2}$ binding energy slightly above 1022 eV and the Zn Auger parameter calculated with the $L_3M_{45}M_{45}$ transition around 2010 eV corresponded well to the reported values for ZnO (1021.4-1022.5 eV and 2009.9-2011.0 eV, respectively) [38,39]. The Auger parameter for $Zn(OH)_2$ was at a lower value, around 2009 eV.

In Figure 10 representative Pt 4f spectra of the calcined and the used Pt/Ga-Zn-oxynitride samples were compared. As discussed previously, the most intense contribution of the calcined samples resulted from Pt^{2+} ions, whereas calcination also resulted in appearance of a small metallic signal. On the other hand, despite the air exposure, the main component of the used samples was the metallic contribution, suggesting a complete reduction of Pt during the photocatalytic reaction. The binding energy of the metallic component was smaller by several tenths of an eV than the literature value for Pt (71.2 eV [38,39]) in all used samples, which indicated a very electron-rich environment for Pt, probably due to effective electron transfer by the oxyhydroxide from the semiconductor particle.

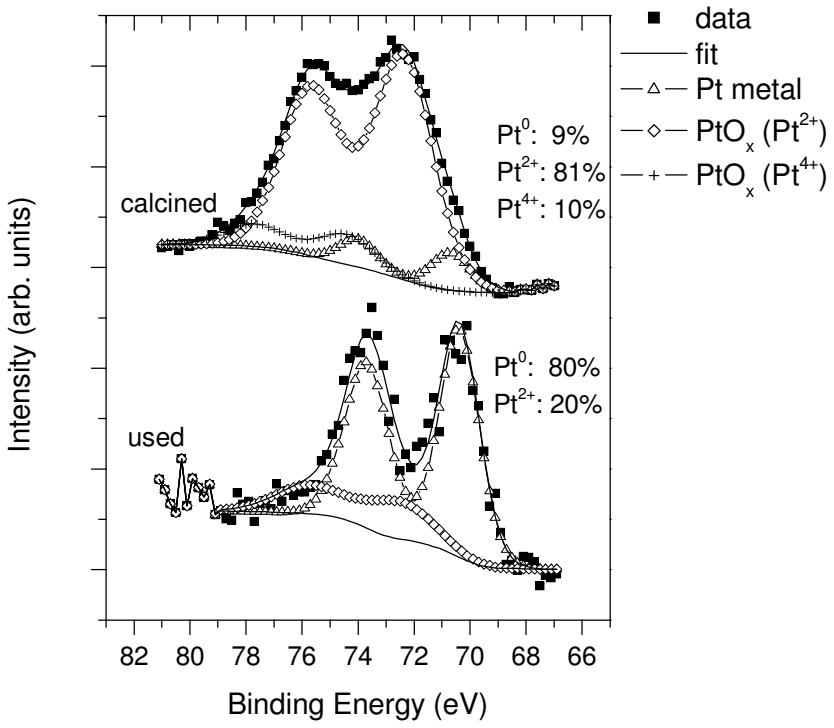

Figure 10. Pt 4f spectra of a calcined and a used Pt/Ga-Zn-oxynitride sample obtained from nitridation of the oxide mixture. Zn/Ga_{nom}=0.14; Pt content= 1 w%.

In Figure 11 the time dependence of the detected hydrogen signal was compared in the initial period of the photocatalytic experiment for the calcined and reduced Pt/Ga-Zn-oxynitride photocatalysts obtained from the oxide mixture. When the co-catalyst was formed by high temperature hydrogen reduction, the starting value of the hydrogen production curve was higher than that in the calcined system, but the hydrogen evolution saturated after less than 1 h. In the case of the calcined photocatalyst the slower activation was accompanied by a notably higher final hydrogen evolution rate.

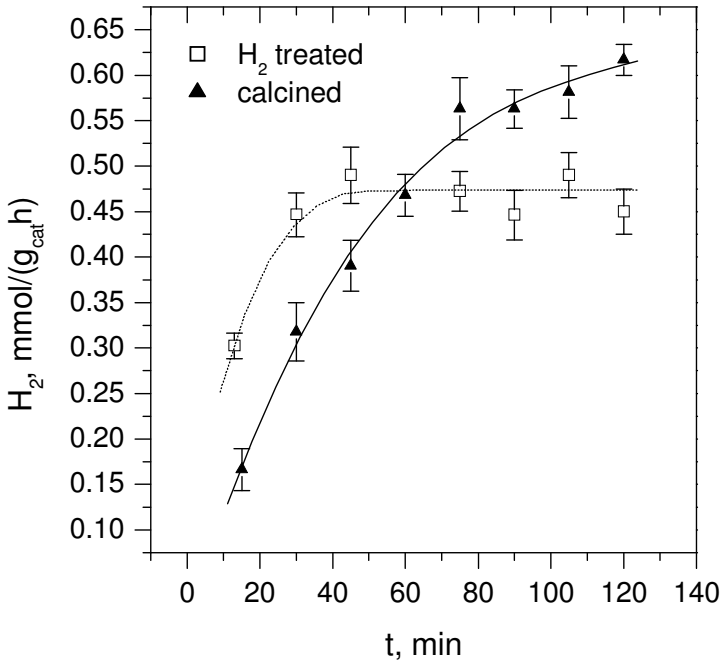

Figure 11. Influence of the Pt co-catalyst formation method on the initial period of the hydrogen production reaction. The Ga-Zn-oxyinitride was obtained from oxide mixture; Zn/Ga_{nom}=0.14. Lines are only guides to the eye.

The gradual increase of the measured hydrogen production implied that the methanol solution should have been first saturated by hydrogen and equilibrium for the liquid phase/nitrogen flow should have been reached before the measurement became relevant to real gas evolution. As this process equally occurred for both photocatalysts, the different initial H_2 release should have been attributed to the interplay of other reasons: (i) transformation of the photocatalyst from the oxynitride into an oxyhydroxide material and (ii) gradual reduction of the initially partially oxidized Pt co-catalyst under the reaction conditions until a steady state is reached.

As the oxynitride-to-oxyhydroxide transformation seemed to require water and leads to nitrogen loss from the system, it was reasonable to assume that the transformation was accompanied by release of gaseous hydrogen and nitrogen. N_2 formation was reported in Ref. [9,29,56,57] in the initial part of the photocatalytic reaction over GaN-ZnO solid solution-based photocatalysts. According to the results discussed above, only the photocatalysts activated by reduction were free from the oxyhydroxide phase prior to the photocatalytic reaction, therefore initially they contain more oxynitride available for the reaction-induced

transformation, which eventually meant a surplus hydrogen source to the methanol photocatalytic reforming process.

Additionally, it was demonstrated that the initially partially oxidized Pt co-catalyst underwent gradual reduction under the reaction conditions until a steady state was reached. The change in the oxidation state of Pt was more pronounced for samples submitted to oxidative treatment. The smaller initial activity of the calcined sample should have therefore partly been due to the more oxidized state of the co-catalyst (Figure 5). However, Figure 11 suggested that the calcined sample provided more preferable conditions for the *in situ* development of the catalytic ensemble (i.e. the interplay between the state of the Pt, the extent of the transformation towards oxyhydroxide and the coupling between the metallic Pt and the semiconducting particle), whereas the reductive pretreatment led to a less favorable situation.

4. Conclusion

In Figure 12 a graphical summary of this study is shown.

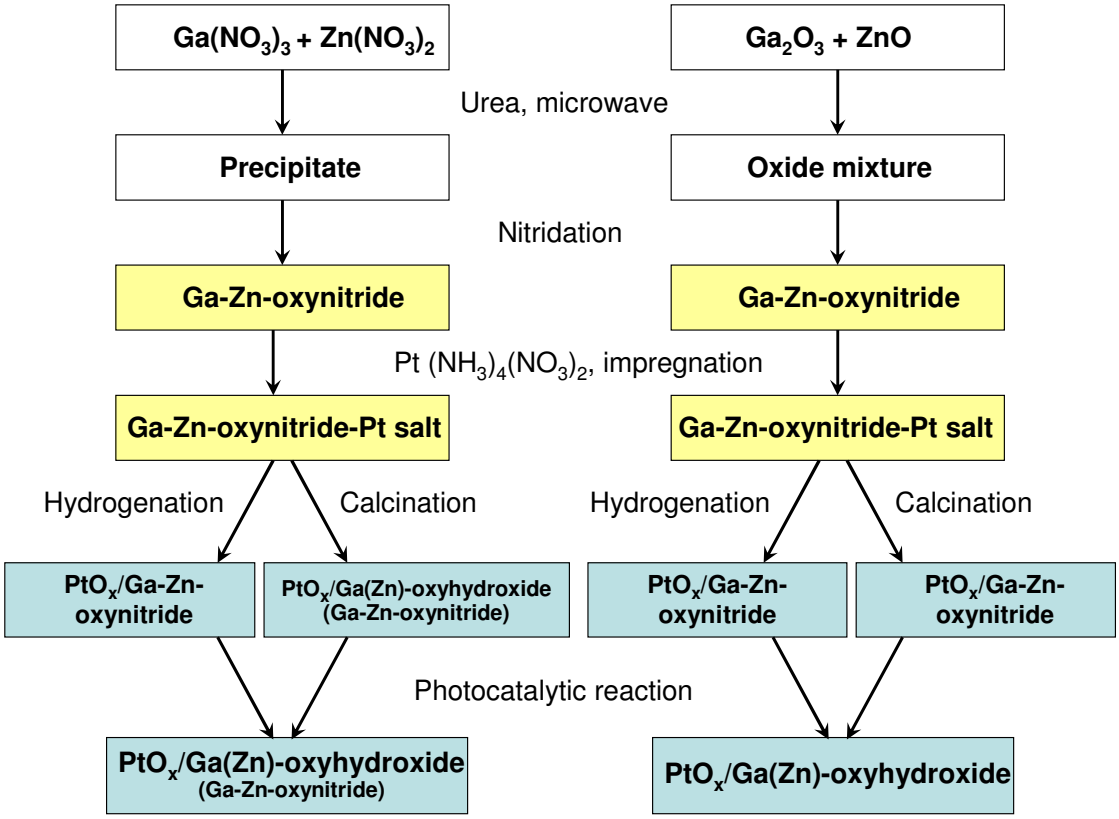

Figure 12. Evolution of the investigated samples during their lifetime.

Ga-Zn-based photocatalysts were prepared by high temperature nitridation of either Ga-Zn-hydroxide-like precipitates obtained from nitrates or mixtures of Ga_2O_3 and ZnO. A

combination of bulk and surface characterization methods revealed that irrespective to the starting material, the product of the synthesis was a wurtzite-like Ga-Zn-oxynitride phase. After synthesis, a Pt co-catalyst was added by impregnation. The oxynitride turned out to be an unstable phase in the presence of Pt: depending on the microstructural properties, at certain stages of the Pt loading and thermal activation it started to transform into a nitrogen-free Ga-Zn-oxyhydroxide. This transformation became complete during the photocatalytic methanol reforming reaction, accompanied by reduction of the Pt co-catalyst until the fully metallic state. Eventually, it was demonstrated that Pt was an effective catalyst in surface transformation of the oxynitride to oxyhydroxide both by thermal and photo activated processes.

The finding that, irrespectively to synthesis routes of the photocatalyst, metallic Pt-loaded Ga-Zn-oxyhydroxide formed under the reaction conditions suggests that this Pt-oxyhydroxide system could play an important role in the photocatalytic reaction. The detailed investigation of this phenomenon is in progress in our lab.

Acknowledgement

This project has been supported by the National Development Agency, grant No. KTIA_AIK_12-1-2012-0014. Financial support by the OTKA-project K77720 (András Tompos) and K100793 (Zoltán Pászti) is greatly acknowledged. Szabolcs Bálint and Péter Németh acknowledge support from János Bolyai Research Fellowship. The authors thank Ms. Ildikó Turi for the technical assistance.

References

[1] L. P. Bicelli, Hydrogen: a clean energy source, Int. J. Hydr. Energy 11 (1986) 555–565.

[2] G. L. Chiarello, M. H. Aguirre, E. Selli, Hydrogen production by photocatalytic steam reforming of methanol on noble metal-modified TiO_2, J. Catal. 273 (2010) 182–190.

[3] S. Kikkawa, K. Nagasaka, T. Takeda, M. Bailey, T. Sakurai, Y. Miyamoto, Preparation and lithium doping of gallium oxynitride by ammonia nitridation via a citrate precursor route, J. Solid State Chemistry 180 (2007) 1984–1989.

[4] A. Miyaake, Y. Masubuchi, T. Takeda, S. Kikkawa, Indium and gallium oxynitrides prepared in the presence of Zn^{2+} by ammonolysis of the oxide precursors obtained via the citrate route, Mater. Res. Bull. 45 (2010) 505–508.

[5] C.C. Hu, H. Teng, Gallium oxynitride photocatalysts synthesized from $Ga(OH)_3$ for water splitting under visible light irradiation, J. Phys. Chem. C, 114 (2010) 20100–20106.

[6] Y. Moriya, T. Takata, K. Domen, Recent progress in the development of (oxy)nitride photocatalysts for water splitting under visible-light irradiation, Coordination Chemistry Reviews, 257 (2013) 1957–1969.

[7] C.C. Hu, Y.L. Lee, H. Teng, Influence of indium doping on the activity of gallium oxynitride for water splitting under visible light irradiation, J. Phys. Chem. C 115 (2011) 2805–2811.

[8] K. Maeda, K. Domen, Solid solution of GaN and ZnO as a stable photocatalyst for overall water splitting under visible light, Chem. Matter, 22 (2010) 612–623.

[9] K. Maeda, K. Teramura, T. Takata, M. Hara, N. Saito, K. Toda, Y. Inoue, H. Kobayashi, K. Domen, Overall water splitting on $(Ga_{1-x}Znx)(N_{1-x}O_x)$ solid solution photocatalyst: Relationship between physical properties and photocatalytic activity, J. Phys. Chem. B. 109 (2005) 20504–20510.

[10] J. Kou, Z. Li, Y. Guo, J. Gao, M. Yang, Z. Zou, Photocatalytic degradation of polycyclic aromatic hydrocarbons in GaN:ZnO solid solution-assisted process: Direct hole oxidation mechanism, J. Mol. Catal. A: Chemical 325 (2010) 48–54.

[11] M.J. Ward, W.Q. Han, T.K. Sham, Nitridation temperature effects on electronic and chemical properties of $(Ga_{1-x}Zn_x)(N_{1-x}O_x)$ solid solution nanocrystals, J. Phys. Chem. C 117 (2013) 20332–20342.

[12] R.M. Navarro, F. del Valle, J.L.G Fierro, Photocatalytic hydrogen evolution from CdS–ZnO–CdO systems under visible light irradiation: effect of thermal treatment and presence of Pt and Ru co-catalysts, Int. J. Hydrogen Energy 33 (2008) 4265–4273.

[13] J. Yang, D. Wang, H. Han, C. Li, Roles of co-catalysts in photocatalysis and photoelectrocatalysis, Acc. Chem. Res. 46 (2013) 1900–1909.

[14] A.L. Linsebigler, G. Lu, T. Yates, Jr, Photocatalysis on TiO_2 surfaces: principles, mechanisms, and selected results, Chem. Rev. 95 (1995) 735–758.

[15] K. Shimura, K. Maeda, H. Yoshida, Thermal acceleration of electron migration in gallium oxide photocatalysts, J. Phys. Chem. C 115 (2011) 9041-9047.

[16] A. Naldoni, M. D'Arienzo, M. Altomare, M. Marelli, R. Scotti, F. Morazzoni, E. Selli, V. Dal Santo, Pt and Au/TiO_2 photocatalysts for methanol reforming: Role of metal nanoparticles in tuning charge trapping properties and photoefficiency, Appl. Catal. B: Environmental 130-131 (2013) 239–248.

[17] J.J. Zou, C. Chen, C.J. Liu, Y.P. Zhang, Y. Han, L. Cui, Pt nanoparticles on TiO_2 with novel metal–semiconductor interface as highly efficient photocatalyst, Materials Letters 59 (2005) 3437–3440.

[18] Q. Gu, J. Long, H. Zhuang, C. Zhang, Y. Zhou, X. Wang, Ternary Pt/SnO_x/TiO_2 photocatalysts for hydrogen production: Consequence of Pt sites for synergy of dual co-catalysts, Phys. Chem. Chem. Phys. 16 (2014) 12521-12534.
[19] S. Trasatti, Work function, electronegativity, and electochemical behaviour of metals. III. Electrolytic hydrogen evolution in acidic solutions, J. Electroanal. Chem. 39 (1972) 163–184.
[20] A. Wood, M. Giersig, P. Mulvaney, Fermi level equilibration in quantum dot-metal nanojunctions, J. Phys. Chem. B 105 (2001) 8810–8815.
[21] J.P. Best, D.E. Dunstan, Nanotechnology for photolytic hydrogen production: Colloidal anodic oxidation (review), Int. J. Hydrogen Energy 34 (2009) 7562–7578.
[22] B. Kraeutler, A.J. Bard, Heterogeneous photocatalytic preparation of supported catalysts. Photodeposition of platinum on TiO_2 powder and other substrates, J. Am. Chem. Soc. 100 (1978) 4317–4318.
[23] H. Einaga, M. Harada, S. Futamura, T. Ibusuki, Generation of active sites for CO photooxidation on TiO_2 by platinum deposition, J. Phys. Chem. B 107 (2003) 9290–9297.
[24] S. Schafer, S.A. Wyrzgol, R. Caterino, A. Jentys, S.J. Schoell, M. Havecker, A. Knop-Gericke, J.A. Lercher, I.D. Sharp, M. Stutzmann, Platinum nanoparticles on gallium nitride surfaces: Effect of semiconductor doping on nanoparticle reactivity, J. Am. Chem. Soc. 134 (2012) 12528–12535.
[25] Z. Jiang, W. Shangguan, Rational removal of stabilizer-ligands from platinum nanoparticles supported on photocatalysts by self-photocatalysis degradation, Catal. Today 242 (2015) 372–380.
[26] T. Ikeda, A. Xiong, T. Yoshinaga, K. Maeda, K. Domen, T. Teranishi, Polyol synthesis of size-controlled Rh nanoparticles and their application to photocatalytic overall water splitting under visible light, J. Phys. Chem. C 117 (2013) 2467–2473.
[27] K. Maeda, K. Teramura, N. Saito, Y. Inoue, K. Domen, Improvement of photocatalytic activity of $(Ga_{1-x}Zn_x)(N_{1-x}O_x)$ solid solution for overall water splitting by co-loading Cr and another transition metal, J. Catal. 243 (2006) 303–308.
[28] K. Maeda, K. Teramura, K. Domen, Effect of post-calcination on photocatalytic activity of $(Ga_{1-x}Zn_x)(N_{1-x}O_x)$ solid solution for overall water splitting under visible light, J. Catal. 254 (2008) 198–204.
[29] K. Maeda, K. Teramura, H. Masuda, T. Takata, N. Saito, Y. Inoue, K. Domen, Efficient overall water splitting under visible-light irradiation on $(Ga_{1-x}Zn_x)(N_{1-x}O_x)$ dispersed with Rh-Cr mixed-oxide nanoparticles: Effect of reaction conditions on photocatalytic activity, J. Phys. Chem. B 110 (2006) 13107–13112.

[30] X. Sun, K. Maeda, M. Le Faucheur, K. Teramura, K. Domen, Preparation of $(Ga_{1-x}Zn_x)(N_{1-x}O_x)$ solid-solution from $ZnGa_2O_4$ and ZnO as a photo-catalyst for overall water splitting under visible light, Appl. Catal. A: General 327 (2007) 114–121.

[31] K. Maeda, H. Hashiguchi, H. Masuda, R. Abe, K. Domen, Photocatalytic activity of $(Ga_{1-x}Zn_x)(N_{1-x}O_x)$ for visible-light-driven H_2 and O_2 evolution in the presence of sacrificial reagentst, J. Phys. Chem. C 112 (2008) 3447–3452.

[32] M. Che, O. Clause, C. Marcilly, 4.1 Deposition of active component, in: G. Ertl, H. Knözinger, J. Weitkamp (Eds.), Preparation of Solid Catalysts, Wiley-VCH, Weinheim, 1999, pp. 315-371.

[33] K. Maeda, K. Teramura, D. Lu, N. Saito, Y. Inoue, K. Domen, Noble-metal/Cr_2O_3 core/shell nanoparticles as a co-catalyst for photocatalytic overall water splitting, Angew. Chem. Int. Ed. 45 (2006) 7806–7809.

[34] C.C. Surdu-Bob, S.O. Saied, J. Sullivan, Surface compositional changes in GaAs subjected to argon plasma treatment, Appl. Surf. Sci. 183 (2001) 126–136.

[35] N. Fairley, www.casaxps.com, 2006.

[36] M. Mohai, XPS MultiQuant: Multimodel XPS Quantification Software, Surf. Interface Anal. 36 (2004) 828–832.

[37] M. Mohai, XPS MultiQuant: Multi-model X-ray photoelectron spectroscopy quantification program, Version 3.00.16 (2003) http://www.chemres.hu/aki/XMQpages/XMQhome.htm.

[38] C.D. Wagner, A.V. Naumkin, A. Kraut-Vass, J.W. Allison, C.J. Powell, J.R. Rumble Jr., NIST X-ray Photoelectron Spectroscopy Database, Version 3.4, National Institute of Standards and Technology, Gaithersburg, MD 2003; http://srdata.nist.gov/xps/.

[39] J.F. Moulder, W.F. Stickle, P.E. Sobol, K.D. Bomben, Handbook of X-ray Photoelectron Spectroscopy, Perkin-Elmer Corp. Eden Prairie, Minnesota, USA, 1992.

[40] L.S. Al-Mazroai, M. Bowker, P. Davies, A. Dickinson, J. Greaves, D. James, L. Millard, The photocatalytic reforming of methanol, Catal. Today 122 (2007) 46–50.

[41] V. Matolin, S. Fabík, J. Glosík, J. Bideux, Y. Ould-Metidji, B. Gruzza, Experimental system for GaN thin films growth and in situ characterization by electron spectroscopic methods, Vacuum 76 (2004) 471–476.

[42] S.D. Wolter, J.M. Delucca, S.E. Mohney, R.S. Kern, C.P. Kuo, An investigation into the early stages of oxide growth on gallium nitride, Thin Solid Films 371 (2000) 153–160.

[43] P. Hill, J. Lu, L. Haworth, D.I. Westwood, J.E. Macdonald, An XPS study of the effect of nitrogen exposure time and temperature on the GaAs(001) surface using atomic nitrogen, Appl. Surf. Sci. 123-124 (1998) 126–130.

[44] I. Bertóti, Characterization of nitride coatings by XPS, Surf. Coat. Techn. 151-152 (2002) 194–203.

[45] D. Selvanathan, F.M. Mohammed, J.O. Bae, I. Adesida, K.H.A. Bogart, Investigation of surface treatment schemes on n-type GaN and $Al_{0.20}Ga_{0.80}N$, J. Vac. Sci. Technol. B 23 (2005) 2538–2544.

[46] Y. Kang, Deposition and characterization of amorphous GaN films, PhD Thesis, Ohio University, 2002.

[47] S. Pal, R. Mahapatra, S.K. Ray, B.R. Chakraborty, S.M. Shivaprasad, S.K. Lahiri, D.N. Bose, Microwave plasma oxidation of gallium nitride, Thin Solid Films 425 (2003) 20–23.

[48] M.F. Pye, J.J. Birtill, P.G. Dickens, α-Gallium oxide deuteriohydroxide: a powder neutron diffraction investigation, Acta Cryst. B33 (1977) 3224–3226.

[49] M. Muruganandham, R. Amutha, M.S.M.A Wahed, B. Ahmmad, Y. Kuroda, R.P.S. Suri, J.J. Wu, M.E.T. Sillanpaa, Controlled fabrication of α-GaOOH and α-Ga_2O_3 self-assembly and its superior photocatalytic activity, J. Phys. Chem. C 116 (2012) 44–53.

[50] J.M. Epp, J.G. Dillard, Effect of ion bombardment on the chemical reactivity of gallium arsenide (100), Chem. Mater. 1 (1989) 325–330.

[51] V. Matolín, I. Matolínová, M. Václavu, I. Khalakhan, M. Vorokhta, R. Fiala, I. Piŝ, Z. Sofer, J. Poltierová-Vejprarová, T. Mori, V. Potin, H. Yoshikawa, S. Ueda, K. Kobayashi, Platinum-doped CeO_2 thin film catalysts prepared by magnetron sputtering, Langmuir 26 (2010) 12824–12831.

[52] F. Şen, G. Gökağac, Different sized platinum nanoparticles supported on carbon: An XPS study on these methanol oxidation catalysts, J. Phys. Chem. C 111 (2007) 5715–5720.

[53] H. Qin, X. Qian, T. Meng, Y. Lin, Z. Ma, Pt/MO_x/SiO_2, Pt/MO_x/TiO_2, and Pt/MO_x/Al_2O_3 catalysts for CO oxidation, Catalysts 5 (2015) 606–633.

[54] H. Xiao, H. Pei, J. Liu, J. Cui, B. Jiang, Q. Hou, W. Hu, Fabrication, characterization, and photocatalysis of GaN–Ga_2O_3 core-shell nanoparticles, Materials Letters 71 (2012) 145–147.

[55] S.P. Phivilay, C.A. Roberts, A.A. Puretzky, K. Domen, Fundamental bulk/surface structure-photoactivity relationships of supported ($Rh_{2-y}Cr_yO_3$)/GaN photocatalysts, J. Phys. Chem. Lett. 4 (2013) 3719–3724.

[56] K. Maeda, H. Masuda, K. Domen, Effect of electrolyte addition on activity of $(Ga_{1-x}Zn_x)(N_{1-x}O_x)$ photocatalyst for overall water splitting under visible light, Catal. Today 147 (2009) 173–178.

[57] K. Kamata, K. Maeda, D. Lu, Y. Kako, K. Domen, Synthesis and photocatalytic activity of gallium–zinc–indium mixed oxynitride for hydrogen and oxygen evolution under visible light, Chem. Phys. Lett. 470 (2009) 90–94.

Table 1. Characteristic binding energies and element ratios obtained from XPS measurements on untreated Ga-Zn-oxynitride samples

Sample	Zn/Ga_{nom}	Ga 3d (eV)	Ga AP[a] (eV)	N 1s (eV)	N/Ga_{XPS}	O 1s (eV)	Zn 2p (eV)	Zn/Ga_{XPS}
Ga_2O_3	--	20.5	1082.7	--	--	531.4	--	--
						533.1		
GaN[b]	--	20.0	1083.5	398.4	0.48	530.8	--	--
						532.4		
Ga-Zn-oxynitride from precipitate	0.32	20.1	1083.3	397.5	0.42	531.3	1022.4	0.19
						532.8		
Ga-Zn-oxynitride from oxides	0.14	20.2	1083.0	397.7	0.37	530.7	1022.2	0.01
						532.3		
Ga-Zn-oxynitride from oxides	0.32	20.1	1083.2	397.8	0.33	530.7	1022.1	0.02
						532.3		

[a]AP= Auger parameter

[b]from Aldrich

Table 2. Change of the Zn/Ga atomic ratios during the high temperature nitridation

N^{o}	Sample preparation	Zn/Ga_{nom}	Zn/Ga_{EDX}	Zn/Ga_{XPS}
1	from precipitate	0.14	0.11	0.09
2*	from precipitate	0.32	0.18	0.19
3*	from precipitate	0.32	0.18	n.d.
4*	from precipitate	0.32	0.19	n.d.
5	from oxides	0.14	0.02	0.01
6	from oxides	0.32	0.03	0.02

*from parallel preparations

Table 3. Characteristic binding energies and element ratios obtained from XPS measurements on 1% Pt-loaded Ga-Zn-oxynitride samples

Sample/co-catalyst formation	Zn/Ga_{nom}	Ga 3d (eV)	Ga AP[a] (eV)	N 1s (eV)	N/Ga ratio	O 1s (eV)	Zn 2p	Zn/Ga ratio	Pt 4f
GaN, Pt calcined	-	20.1	1083.4	397.6	0.49	530.9	--	--	71.4
						532.4			72.4
									74.1
Ga-Zn-oxynitride from precipitate,	0.14	20.2	1082.7	397.6	0.20	531.2	1022.5	0.09	72.8
Pt loaded only incipient wetness						532.5			74.9
									later
									70.9
									72.4
									74.7
Ga-Zn-oxynitride from precipitate,	0.14	20.1	1083.4	397.6	0.45	531.3	1022.3	0.10	71.5
Pt reduced						532.4			72.5
Ga-Zn-oxynitride from precipitate,	0.32	20.2	1083.0	397.6	0.27	531.4	1022.6	0.18	71.4
Pt reduced						532.7			72.6
Ga-Zn-oxynitride from precipitate,	0.14	20.2	1082.5	397.4	0.14	531.3	1022.5	0.17	70.9
Pt calcined						532.5			72.6
Ga-Zn-oxynitride from oxides,	0.14	20.2	1082.8	397.5	0.08	531.2	1022.4	0.02	70.6
Pt calcined						532.6			72.4
Ga-Zn-oxynitride from oxides,	0.14	20.2	1083.1	397.6	0.40	531.3	1022.3	0.01	71.5

Pt hydogenated	532.4	72.6

[a]AP= Auger parameter

Table 4. Characteristic binding energies and element ratios obtained from XPS measurements on the spent Pt-loaded GaN-ZnO photocatalysts

Sample/co-catalyst formation	Zn/Ga_{nom}	Ga 3d (eV)	Ga AP[a] (eV)	N 1s (eV)	N/Ga ratio	O 1s (eV)	Zn 2p	Zn/Ga ratio	Pt 4f
Ga_2O_3, Pt calcined	--	20.2	1082.7	--	--	531.1	--	--	70.8
						532.3			72.4
GaN, Pt calcined	--	20.3	1083.3	397.9	0.35	531.1	--	--	70.9
						532.4			72.2
Ga-Zn-oxynitride from precipitate, Pt reduced	0.32	20.1	1082.8	397.1	0.04	531.2	1022.5	0.20	70.6
						532.5			
Ga-Zn-oxynitride from precipitate,	0.32	20.1	1082.5	397.1	0.04	531.2	1022.5	0.17	70.7
Pt calcined						532.3			
Ga-Zn-oxynitride from oxides,	0.14	20.2	1082.6	--	0.00	531.0	1022.4	0.02	70.4
Pt reduced						532.2			72.1
Ga-Zn-oxynitride from oxides,	0.32	20.3	1082.7	397.5	0.08	531.3	1022.5	0.02	70.8
Pt calcined						532.5			72.3
Ga-Zn-oxynitride from oxides,	0.14	20.1	1082.6	--	0.00	531.0	1022.2	0.04	70.4
Pt calcined						532.2			72.3

aAP= Auger parameter

Supplementary material

S1. XRD measurements

As can be seen in Figure S1 the Zn incorporation into the oxynitride resulted in a slight shift of the positions of the diffraction peaks to lower 2Θ angles comparing to GaN. This phenomenon is an obvious consequence that ionic radius of Zn is larger than that of Ga. Similar observations have been described in details by Maeda et al [S1].

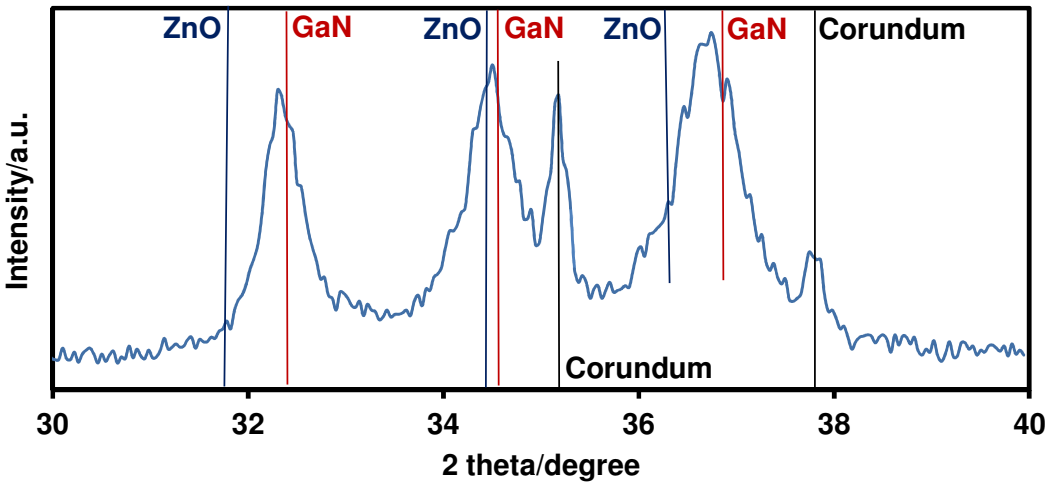

Figure S1. XRD patterns of the Ga-Zn-oxynitride obtained by nitridation of the precipitate from $Zn(NO_3)_2$ and $Ga(NO_3)_3$ at Zn/Ga_{nom}=0.32 (corundum internal standard added)-enlargement of line a in Figure 1 in the main text. Reference cards from ICDD PDF-2 (1998) data base, ZnO (# 36-1451), GaNh (# 76-0703), corundum (# 10-0173).

S2. UV-Visible diffuse reflectance spectroscopic measurements

In order to obtain information on the optical properties of the Ga-oxynitride samples, diffuse reflectance UV-visible spectra were recorded prior to the Pt-loading step. The spectra were registered using a Jasco V-570 UV-VIS spectrophotometer equipped with a NV-470 type integrating sphere. The data were collected between 800 and 200 nm wavelengths. The reflectance data were transformed by means of the Kubelka-Munk function ($F(R) = (1-R)^2/2R$, where R is the measured reflectance [S2]). The Kubelka-Munk function is regarded to be proportional to the absorption coefficient α, thus it represents the approximate wavelength dependence of the absorption coefficient α.

As it is shown in Figure S2, the absorption properties of the samples are determined by the actual Zn content. Samples with low Zn concentration (i.e. those obtained from oxides, regardless to the intended Zn content) give very similar spectra to that of the GaN reference. A more pronounced absorption in the visible region is obtained for the samples obtained from precipitates, for which a representative example is presented.

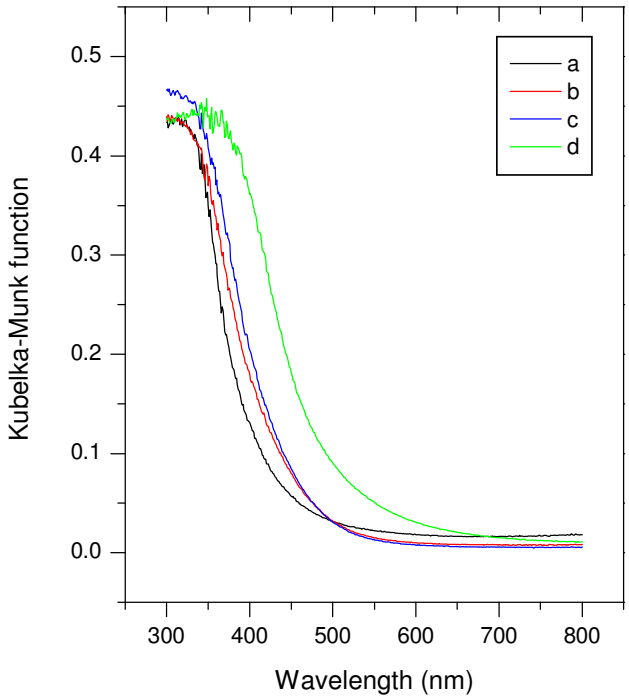

Figure S2. Diffuse reflectance spectra of nitridated samples.
a: commercial GaN, b: from oxide mixtures, Zn/Ga_{nom}=0.14; c: from oxide mixtures, Zn/Ga_{nom}=0.32; d: from precipitate, Zn/Ga_{nom}=0.32.

The absorption spectra can be used for determination of the band gaps of the samples. The evaluation of the band gap values was performed by plotting the quantity $(F(R)E_{photon})^2$ as the function of the photon energy (E_{photon}) (Tauc plots [S3]). In the adsorption edge region the plots were linear, as expected for direct band gap materials; the intersection of the fit to the linear segment with the base line gave the band gap values, as presented in Table S2. The data are in qualitative agreement with those available in the literature [S1, S4].

Table S2. Band gaps of nitridated samples calculated from Kubelka-Munk function

Line in Figure S1	Sample preparation	Zn/Ga_{EDX}	Band gap (eV)
a	GaN	-	3.3
b	from oxide mixture	0.02	3.15
c	from oxide mixture	0.03	3.05
d	from precipitate	0.18	2.8

S3. XPS measurements

The XPS characteristics of selected reduced or calcined Ga-Zn-oxynitrides [Table S2] were essentially undistinguishable from those of the as synthesized materials, confirming that neither reduction nor calcination alters even the surface of the photocatalysts if they are free of Pt.

Table S2. Characteristic binding energies and element ratios obtained from XPS measurements on reduced and calcined GaN-ZnO samples

Sample/ treatment	Zn/Ga_{nom}	Ga 3d (eV)	Ga AP (eV)	N 1s (eV)	N/Ga ratio	O 1s (eV)	Zn 2p	Zn/Ga ratio
GaN, calcined	--	20.1	1083.3	398.3	0.46	530.8 532.8	--	--
Ga-Zn-oxynitride from precipitate, reduced	0.32	20.1	1083.5	397.9	0.41	531.0 532.4	1022.4	0.20
Ga-Zn-oxynitride from precipitate, calcined	0.32	20.3	1083.1	397.7	0.36	531.4 532.9	1022.6	0.17
Ga-Zn-oxynitride from precipitate, calcined	0.14	20.3	1083.	397.8	0.44	531.4 533.0	1022.5	0.09
Ga-Zn-oxynitride from oxides, calcined	0.14	20.1	1083.6	397.9	0.41	531.0 532.4	1022.3	0.04

As a typical example for the changes of the Ga 3d core level during the life cycle of the (Ga, Zn)-oxynitride photocatalysts, in Figure S3.1 spectra collected from the oxide-derived sample with $Zn/Ga_{nom}=0.32$ are compared to those measured on GaN and Ga_2O_3. As discussed in the main text, the change of the binding energy of the Ga 3d peak is rather small during transition from the oxynitride to the oxyhydroxide state.

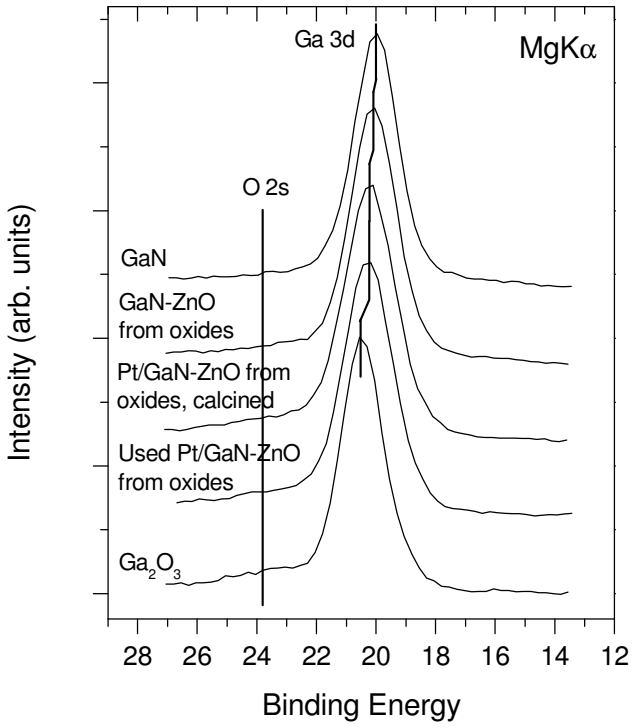

Figure S3.1. Ga 3d spectra of Ga-Zn-oxynitride prepared from oxides ($Zn/Ga_{nom}=0.32$) after nitridation, after Pt loading and calcination and after the photocatalytic experiment, compared to those of GaN and Ga_2O_3.

The Ga Auger parameter calculated as the sum of the binding energy of the Ga 3d band and the kinetic energy of the Ga $L_3M_{45}M_{45}$ Auger peak is a much more sensitive indicator of the changes in the chemical environment of the Ga atoms. In Figure S3.2 Auger parameter values measured on the oxide-derived with $Zn/Ga_{nom}=0.32$ sample at certain stages of the life cycle are compared to those measured on GaN and Ga_2O_3. As mentioned in the main text, the measured Ga Auger parameter of GaN is significantly lower than the literature value, due to surface oxidation of the crystallites. The as prepared oxynitride exhibits a somewhat smaller Auger parameter, which further decreases upon Pt loading and calcination, indicating the onset of the structural transformation. In the case of the recovered catalyst, the very low Auger parameter points to a heavily oxidized environment for Ga.

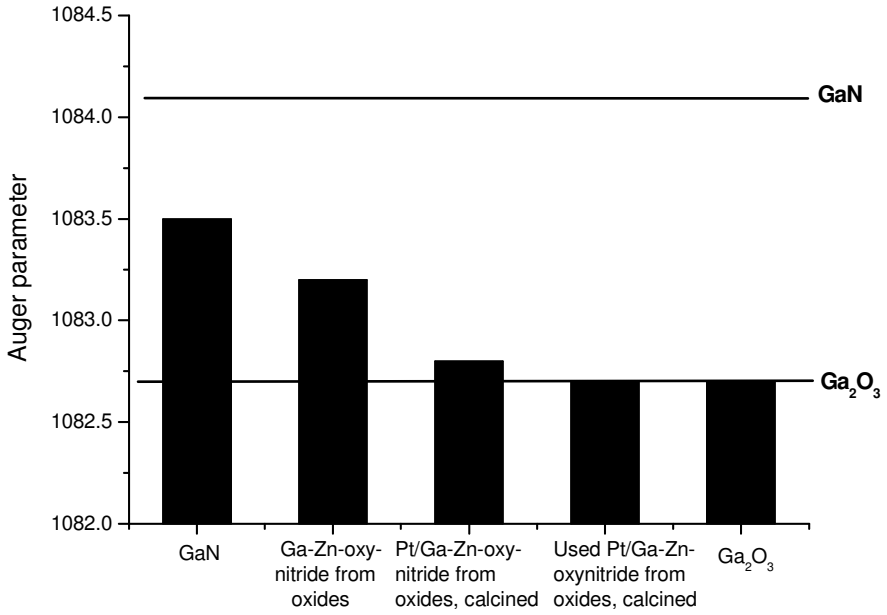

Figure S3.2. Auger parameter data for Ga-Zn-oxynitride prepared from oxides (Zn/Ga_{nom}=0.32) after nitridation, after Pt loading and calcination and after the photocatalytic experiment, compared to those for GaN and Ga_2O_3.

References:

[S1] K. Maeda, K. Teramura, T. Takata, M. Hara, N. Saito, K. Toda, Y. Inoue, H. Kobayashi, K. Domen, J. Phys. Chem. B 109 (2005) 20504-20510.

[S2] G.A. Klein, Industrial color physics, Springer Series in Optical Sciences 154, Chapter 5, Springer, 2010

[S3] S. Kasap, P. Capper (Eds.), Springer Handbook of Electronic and Photonic Materials, Chapter 3, Springer, 2006.

[S4] K. Maeda, H. Hashiguchi, H. Masuda, R. Abe, K. Domen, J. Phys. Chem. C 112, (2008) 3447-3452.